Thymic macrophages consist of two populations with distinct localization and origin

Tyng-An Zhou[1], Hsuan-Po Hsu[1], Yueh-Hua Tu[2,3], Chih-Yu Lin[1], Nien-Jung Chen[1], Jin-Wu Tsai[4], Ellen A. Robey[5], Hsuan-Cheng Huang[2,6], Chia-Lin Hsu[1], and Ivan L. Dzhagalov[1*]

[1]Institute of Microbiology and Immunology, National Yang-Ming University, Taipei, Taiwan

[2]Bioinformatics Program, Taiwan International Graduate Program, Institute of Information Science, Academia Sinica, Taipei, Taiwan

[3]Graduate Institute of Biomedical Electronics and Bioinformatics, National Taiwan University, Taipei, Taiwan

[4]Brain Research Center, National Yang-Ming University, Taipei, Taiwan

[5]Division of Immunology and Pathogenesis, Department of Molecular and Cell Biology, University of California, Berkeley, CA, United States

[6]Institute of Biomedical Informatics, National Yang-Ming University, Taipei, Taiwan

*Correspondence to Ivan L. Dzhagalov: ivan.dzhagalov@nycu.edu.tw, ORCID: 0000-0001-9209-4582

Mailing Address: Ivan L. Dzhagalov, Institute of Microbiology and Immunology, National Yang-Ming Chiao-Tung University, #155, Sec. 2, LiNong Street, Beitou, Taipei City, 11221, TAIWAN

Abstract

Tissue-resident macrophages are essential for protection from pathogen invasion and maintenance of organ homeostasis. The ability of thymic macrophages to engulf apoptotic thymocytes is well appreciated, but little is known about their ontogeny, maintenance, and diversity. Here, we characterized the surface phenotype and transcriptional profile of these cells and found out that they express typical tissue-resident macrophage genes yet also exhibit organ-specific features. Thymic macrophages were most closely related to spleen red pulp macrophages and Kupffer cells and shared the expression of the transcription factor SpiC with these cells. Using shield chimeras, transplantation of embryonic thymuses, and fate mapping, we found that three distinct waves of precursors generate thymic macrophages. Moreover, some of them proliferated in situ. Single-cell RNA sequencing showed that the macrophages in the adult thymus are composed of two populations with distinct localization and origin. Altogether, our work defines the phenotype, origin, and diversity of thymic macrophages.

Introduction

Tissue-resident macrophages are present in every organ and maintain local homeostasis through diverse functions ranging from protection against pathogens to tissue repair[1]. To perform their roles efficiently, macrophages acquire specialized phenotypes depending on the tissue microenvironment, and as a consequence, multiple subtypes exist, frequently within the same organ. For example, the spleen harbors red pulp macrophages specialized in red blood cell phagocytosis, marginal zone macrophages and metallophilic macrophages that are the first defense against blood-borne pathogens, T cell zone macrophages that silently dispose of apoptotic immune cells, and tingible-body macrophages that engulf less fit B cells in the germinal center[2-4]. Thus, tissue-resident macrophages represent a fascinating developmental system that allows enormous plasticity.

The last decade has seen a paradigm shift in our understanding of the development of tissue-resident macrophages. Contrary to the long-held belief that all macrophages derive from circulating monocytes[5], multiple studies have shown that many of them are long-lived cells with an embryonic origin that can maintain themselves in the tissues (reviewed in[6]). Three waves of distinct progenitors settle the tissues and contribute in various degrees to the resident macrophages in each organ. The first wave consists of yolk sac (YS)-derived primitive macrophages that enter all tissues and establish the earliest macrophage populations[7,8]. In all organs, except for the brain and, partially, the epidermis, primitive macrophages are replaced by the next wave consisting of fetal monocytes[9-12]. The third wave comes from hematopoietic stem cell (HSC)-derived monocytes that contribute to various degrees to the

macrophage pool in different tissues. For example, these cells contribute little to the microglia in the brain, Langerhans cells in the epidermis, and alveolar macrophages in the lungs but substantially to most other organs[13-16]. Moreover, the kinetics and timing of HSC-derived monocytes infiltration vary in different parts of the body. For some macrophage populations, such as the arterial macrophages and subcapsular lymph node macrophages, monocytes replace embryonic macrophages soon after birth and self-maintain after that with little contribution from circulating cells[17,18]. Others, such as heart macrophages, osteoclasts, and pancreatic isles macrophages are progressively replaced at a low rate[14,19-23]. A third group, such as the macrophages in the dermis and most of the gut macrophages, are constantly replaced by blood monocytes with relatively fast kinetics[24,25]. These conclusions have been extended to many different macrophage populations such as Kupffer cells, liver capsular macrophages, red pulp macrophages, testicular macrophages, large and small peritoneal macrophages, and T zone macrophages in the lymph nodes[2,13,14,16,26-30].

The recent revitalization in macrophage research has yet to reach thymic macrophages. Although their prodigious phagocytic ability is well appreciated[31], little is known about the origin, diversity, and maintenance of these cells. This gap in our knowledge is, in part, due to the lack of a consensus about the surface phenotype of thymic macrophages. Various groups have used different markers to identify these cells, such as F4/80 and Mac-3 (LAMP-2)[31], or CD4 and CD11b[32], or Mac-2 (galectin 3), F4/80 and ED-1 (CD68)[33]. Most commonly, researchers employ F4/80 and CD11b[34-37]. However, none of these markers is macrophage-specific: F4/80 is also

expressed on eosinophils and monocytes[38,39], while CD11b is present on most myeloid cells. The lack of a clear phenotypic definition of thymic macrophages has translated into the absence of models that target genes specifically in this population. For example, although macrophages in various organs have been successfully targeted with *Lyz2*^{Cre}, *Csf1r*^{Cre}, or *Cx3cr1*^{Cre}, very few studies have used these models in the thymus[37,40,41].

Only a handful of studies has explored the origin of thymic macrophages. Several reports have indicated that these cells could be derived from T cell progenitors in the thymus based on an improved single cell in vitro culture and in vivo transplantation experiments[42,43]. However, these conclusions have been questioned based on fate-mapping experiments using *Il7r*^{Cre} that found very limited contribution of lymphoid progenitors to thymic macrophages in vivo in unperturbed mice[44]. Most recently, Tacke et al. used parabiosis to rule out circulating monocytes as a major source for thymic macrophages[37]. The same study also performed fate-mapping experiments to show that most thymic macrophages descend from *Flt3*$^{+}$ HSC-derived progenitors. However, the contribution of earlier waves of hematopoiesis has not been explored.

Here, we aimed to bring our knowledge of thymic macrophages on par with other tissue-resident macrophages. We started by providing a clear definition of thymic macrophages according to the guidelines set by the Immunological Genome Consortium (IMMGEN)[38] and characterized their surface phenotype and transcriptional signature. Using single-cell RNA sequencing (scRNA-Seq), we identified two populations of thymic macrophages with distinct localization. We explored the origin of these cells through genetic fate mapping, shield chimeras, and embryonic thymus transplantation and

documented that three separate waves of progenitors give rise to resident thymic macrophages. Altogether our work fills an important gap in our understanding of resident thymic macrophages and provides the framework for future functional characterization of these cells.

Results:

CD64, F4/80, and MerTK identify the macrophages in the thymus

To unambiguously and comprehensively identify macrophages in the thymus, we evaluated several of the prototypical macrophage markers, MerTK, CD64, and F4/80[38]. Only MerTK identified a population that stained completely with the other two markers (Fig. 1a). F4/80 labeled Siglec F^+SSC^{hi} eosinophils and $CD64^+CD11b^+$ monocytes, in addition to $MerTK^+$ cells (Fig. S1a). CD64 identified $CD11b^+F4/80^{lo}$ monocytes (Fig. S1b). Thus, MerTK appeared to be the best marker for macrophages in the thymus. However, staining with MerTK and F4/80 was relatively dim even when the brightest fluorochromes (e.g., PE) were used and could not be resolved fully from the isotype control (Fig. S1c). For practical purposes, to identify macrophages, we used CD64 together with F4/80 and CD11b to exclude monocytes (Fig. S1d). In addition, we also employed forward scatter (cells size) to exclude cells that appeared $MerTK^+$, $CD64^+$, $F4/80^+$, but were much smaller and less granular than the rest of the macrophages, and many of them were $Thy1^+$ (Fig. S1e).

The $CD64^+F4/80^+MerTK^+CD11b^{lo}FSC^{hi}$ cells had typical macrophage morphology with abundant cytoplasm (Fig. 1b). These cells did not express lineage markers characteristic of T cells (CD3ε), B cells (CD19), eosinophils

(Siglec F), NK cells (NK1.1), neutrophils (Gr1), or plasmacytoid dendritic cells (Siglec H) (Fig. 1c). However, they expressed phagocytic receptors such as TIM4, CD51, and Axl (Fig. 1d).

To ascertain that our gating strategy identifies all macrophages in the thymus in an unbiased way, we performed scRNA-Seq of sorted *Csf1r*$^{GFP+}$ and *Cd11c*$^{YFP+}$ thymic cells. *Csf1r* is required for the survival of most macrophages and is considered their definitive marker[45,46], while *Cd11c*^{YFP} is expressed in many myeloid cells, including macrophages[47]. Both reporters identified an overlapping set of cells (Fig. S2a). Two clusters expressed the macrophage/monocytes-specific transcription factor *Mafb* and high levels of *Fcrg1* (CD64), *Mertk*, and *Adgre1* (F4/80), indicating that they are macrophages (Fig. 1e). An additional cluster expressed *Mafb* together with *Fcgr1* and *Adgre1* but not *Mertk*, fitting the description of monocytes. Altogether the scRNA-Seq data confirmed that our flow cytometry gating had identified all macrophages in the thymus. Importantly, MerTK^{+} cells could not be labeled by intravenously injected CD45 antibody (Fig. 1f), proving that they reside in the parenchyma of the organs and not in the blood vessels. Based on the above data, we will refer to CD64^{+}F4/80^{+}MerTK^{+}CD11b^{lo}FSC^{hi} cells as thymic macrophages. The smaller CD64^{+}F4/80^{lo}CD11b^{+}FSC^{hi} population did not express MerTK, but most of them expressed Ly6C, and we classify them as thymic monocytes.

Thymic macrophages expressed CD11c, MHC2, and SIRPα that made them partially overlap with CD11c^{+}MHC2^{+} classical dendritic cells (cDCs), thus making problematic the unambiguous identification of thymic cDCs based only on these two markers (Fig. S1f). Proper identification of cDC in the

thymus requires the exclusion of macrophages based on CD64 or MerTK staining. Otherwise, the cDCs, particularly the SIRPα^+ cDC2 subset, would be contaminated with macrophages that account for ~25% of cDC2 (Fig. S1g).

Thymic macrophages were ~0.1% of all the cells in the thymus of young adult mice and numbered ~4x10^5 on average per mouse (Fig. 1g). We did not find statistically significant differences in their percentages between 4 and 11 weeks of age. Still, there was a significant decline in their numbers with age, consistent with the beginning of thymic involution (Fig. 1h).

To determine if thymic macrophages are avid phagocytes, we evaluated their participation in the phagocytosis of apoptotic cells in the thymus by TUNEL staining. We used TIM4 and MerTK as single stains to identify macrophages in tissue sections because they are not expressed on any other cell type in the thymus instead of following our multiple-label flow cytometry strategy. Most of the TUNEL$^+$ cells could be found clearly inside or closely associated with MerTK$^+$ and TIM4$^+$ cells in the thymus (Fig. S3a and b). On average, ~85% of all TUNEL$^+$ cells were within 5 μm of MerTK$^+$ cells, indicating that thymic macrophages are the major phagocytic population in the thymus (Fig. S3c). The degree of co-localization between TUNEL$^+$ cells and TIM4$^+$ cells was slightly lower, ~75% on average, possibly reflecting the absence of TIM4 expression on a small proportion of thymic macrophages (Fig. 1d).

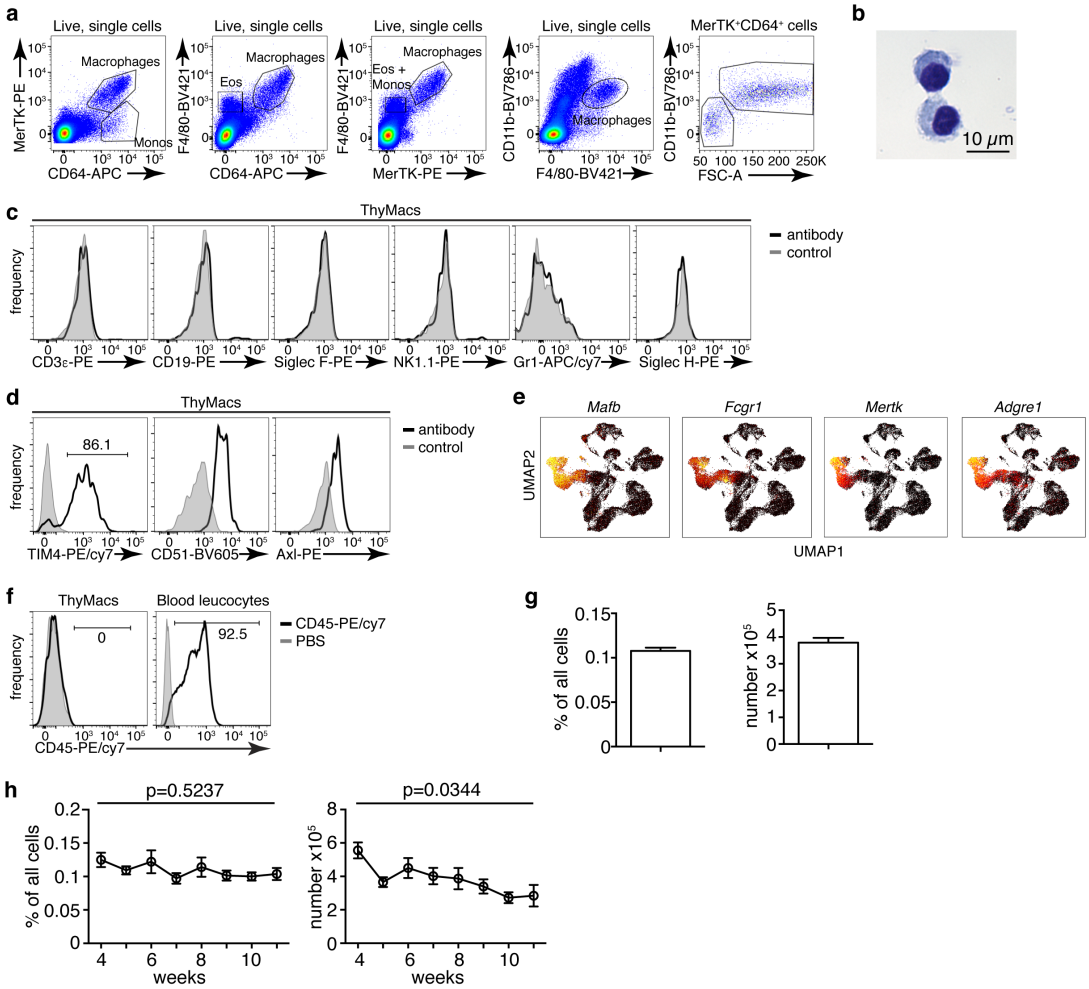

Figure 1. Thymic macrophages (ThyMacs) can be identified by the expression of CD64, MerTK and F4/80. a Flow cytometric analysis of enzymatically digested thymus tissue with macrophage markers CD64, MerTK, F4/80, and CD11b. More details about the confirmation of the identities of eosinophils and monocytes can be found in Fig. S1a and b. **b** Pappenheim (Hemacolor Rapid staining kit) staining of sorted ThyMacs. **c** Lack of expression of lineage markers associated with other cell types on ThyMacs. **d** The expression on ThyMacs of three receptors for phosphatidylserine that participate in the phagocytosis of apoptotic cells. **e** scRNA-Seq data showing the expression of prototypical macrophage genes *Mafb*, *Fcgr1* (CD64), *Mertk*, and *Adgre1* (F4/80) among thymus cells sorted as *Csf1r*$^{GFP+}$ and *Cd11c*$^{YFP+}$. **f** Labeling of ThyMacs with intravenously

injected anti-CD45-PE antibody or PBS. The labeling of blood leucocytes is shown for comparison. **g** Average numbers and percentages of ThyMacs in 4-11 weeks old mice, n=82. **h** Comparison of the numbers and percentages of ThyMacs in mice of different ages, n=82. All flow cytometry plots are representative of at least 3 independent repeats. The numbers in the flow cytometry plots are the percent of cells in the respective gates. Data in **g** and **h** represent mean±SEM. Statistical significance in **h** was determined with one-way ANOVA.

Transcriptional signature of thymic macrophages

To further understand the identity and functions of the thymic macrophages, we sorted and subjected them to RNA sequencing analysis as part of the IMMGEN's Open Source Mononuclear Phagocyte profiling. Thymic macrophages displayed a transcription profile consistent with tissue-resident macrophages and did not express genes characteristic of other lineages (Fig. 2a). Then, we examined the expression of the core signature macrophage genes[38] and found that they were enriched in thymic macrophages but not in *Sirpa*$^{+}$ or *Xcr1*$^{+}$ thymic cDCs (Fig. 2b). On the contrary, cDC core signature genes were abundantly expressed in both thymic cDC subsets but not in thymic macrophages. These findings establish that although thymic macrophages and cDCs share the thymic microenvironment and expression of CD11c and MHC2, they have distinct transcriptional profiles.

We then compared the gene expression profile of thymic macrophages to that of other well-characterized macrophage populations available from

IMMGEN. Because of the abundance of samples, we limited our comparison to only nine types of tissue-resident macrophages under steady-state conditions – splenic red pulp macrophages, Kupffer cells, broncho-alveolar lavage macrophages, large peritoneal cavity macrophages, white adipose tissue macrophages, aorta macrophages, central nervous system microglia, and spinal cord microglia. Hierarchical clustering revealed that thymic macrophages were most closely related to splenic red pulp macrophages and Kupffer cells (Fig. 2c).

To better identify the unique functions of thymic macrophages, we looked for genes that were differentially expressed in these cells compared to other tissue-resident macrophages. We set three criteria: 1) high expression in thymic macrophages (>500); 2) >5 fold higher expression than the average value in the nine populations of non-thymic macrophages; 3) expression in thymic macrophages is higher than any non-thymic macrophage samples. A total of 44 genes met these criteria, and we consider them to constitute the transcriptional signature of thymic macrophages (Fig. 2d). These included several degradation enzymes and their inhibitors (*Cst7*, *Mmp2*, *Mmp14*, *Dnase1l3*, *Serpina3g*, *Acp5*), non-classical MHC molecules (*H2-M2*, *H2-Q6*, *H2-Q7*), metabolic enzymes (*Chst2*, *Ass1*, *Kynu*, *Cp*, *Dgat2*, *Sorl1*, *Lap3*), molecules involved in innate immunity (*Ifit2*, *Il18bp*, *Mefv*, *Lgals3bp*) and extracellular signaling molecules and their receptors (*Pdgfa*, *Cxcl16*, *Il2rg*, *Gpr157*). We also looked for transcription factors (TFs) highly expressed in thymic macrophages and could potentially regulate critical gene networks in these cells. A total of 25 TFs were highly expressed in thymic macrophages (>250) and were at least 2-fold higher as compared to the non-thymic

252 macrophages (Table S1). Among them were several TFs involved in type I
253 interferon (IFN-I) signaling (*Stat1*, *Stat2*, *Irf7*, and *Irf8*) and lipid metabolism
254 (*Nr1h3*, *Pparg*, *Srebf1*, and *Rxra*) (Fig. 2e). Notably, *Runx3* that is important
255 for the development and function of cytotoxic T lymphocytes[48], innate
256 lymphoid cells[49], and Langerhans cells[50] was highly expressed in thymic
257 macrophages. *SpiC* that has well-documented roles in the development of red
258 pulp macrophages in the spleen, and bone marrow macrophages[51,52] was
259 also highly expressed in thymic macrophages, further strengthening the
260 argument for the similarity between thymus, spleen and liver macrophages.
261 To confirm the expression of *Spic* in thymic macrophages, we analyzed the
262 thymus of $Spic^{GFP}$ mice[52]. We found that all $Spic^{GFP+}$ cells were
263 macrophages (Fig. S4a and b), making them the most specific thymic
264 macrophage reporter strain compared with $Lyz2^{GFP}$, MAFIA ($Csf1r^{GFP}$),
265 $Cd11c^{YFP}$, and $Cx3cr1^{GFP}$ mice (Fig. S4c-e). However, only ~80% of thymic
266 macrophages were $Spic^{GFP+}$ suggesting heterogeneity within the cells (Fig.
267 S4f and g).
268 Several dominant pathways emerged when we grouped the 500 most
269 highly expressed genes in thymic macrophages according to gene ontology
270 (GO) terms (Fig. 2f). It was notable that five of the ten most highly enriched
271 GO pathways concerned antigen presentation of both exogenous and
272 endogenous antigens. These data complement our flow cytometry findings of
273 expression of MHC2 and suggest that thymic macrophages could be potent
274 antigen-presenting cells and might play a role in negative selection or agonist
275 selection of thymocytes. Two other highly enriched GO pathways were
276 involved in lysosomal biogenesis and functions, highlighting the high capacity

of these cells to degrade phagocytosed material. Thus, our transcriptional analysis has revealed that thymic macrophages are bona fide macrophages that bear significant similarity to spleen and liver macrophages and are specialized in lysosomal degradation of phagocytosed material and antigen presentation.

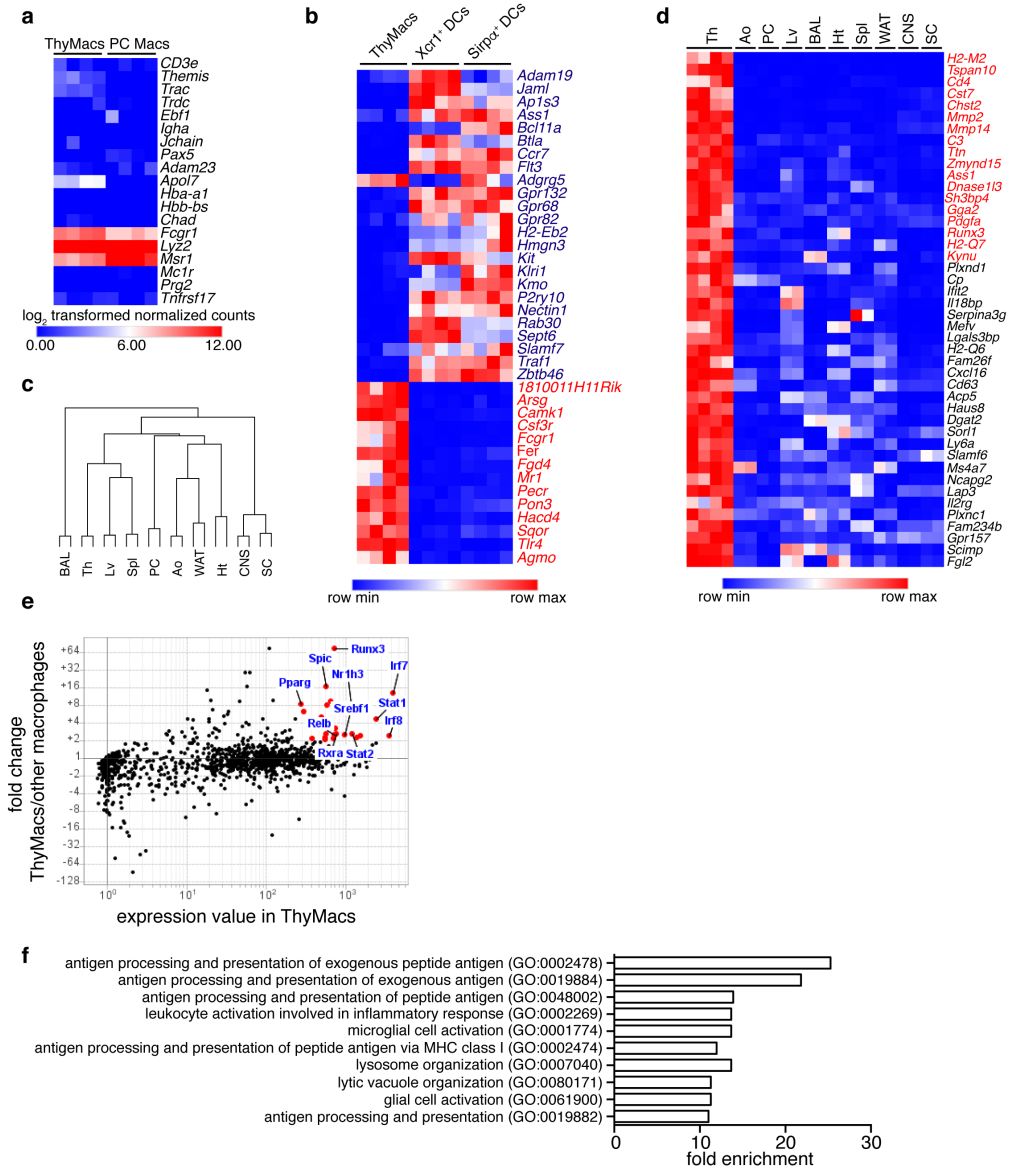

Figure 2. Transcriptional profile of thymic macrophages (ThyMacs). a Expression of lineage-specific genes in ThyMacs and peritoneal cavity macrophages (PC Macs). **b** Expression of cDC-specific genes (gene names in blue) and macrophage-specific genes (gene names in red) in ThyMacs and two populations of thymic cDCs (ThyDCs) – *Xcr1*$^+$ ThyDCs and *Sirpa*$^+$

ThyDCs. **c** Hierarchical clustering of ThyMacs and nine other populations of tissue-resident macrophages in duplicates. **d** Highly expressed (>500) genes enriched (>5-fold) in ThyMacs (4 samples) compared to nine other tissue-resident macrophage populations (two samples each). The genes in red are >10-fold up-regulated in thymic macrophages. **e** Comparison of the geometric mean expression of transcription factors in thymic macrophages (4 samples) and the nine other macrophage populations (2 samples each). Transcription factors with expression >250 and fold change >2 are marked with red dots. **f** Top 10 GO pathways in ThyMacs based on the 500 most highly expressed genes in these cells. Th – ThyMacs, Spl – spleen red pulp macrophages, Lv – Kupffer cells, BAL – bronchoalveolar lavage macrophages, PC – peritoneal cavity macrophages, Ao – aorta macrophages, Ht – heart macrophages, WAT – white adipose tissue macrophages, CNS – central nervous system microglia, SC – spinal cord microglia.

Yolk-sac progenitors contribute to embryonic thymic macrophages

The ontogeny of thymic macrophages has been examined by only one study since the realization that many tissue-resident macrophages are descendants from embryonic progenitors[37]. Based on *Flt3*^{Cre} fate-mapping, the authors concluded that most adult thymic macrophages derive from HSCs. To determine if yolk-sac (YS) progenitors contribute to embryonic thymic macrophages, we used *Cx3cr1*^{CreER} fate mapping[53]. Injection of 4-OHT at E9.5 in *ROSA26*$^{LSL\text{-}GFP}$ mouse mated with a *Cx3cr1*^{CreER} male permanently tags YS progenitors and their descendants with GFP (Fig. 3a). Indeed, E19.5 microglia that are exclusively derived from YS progenitors were

labeled to a high degree (Fig. 3b). After adjusting for incomplete labeling based on the microglia, we found that at E15.5 >50% of thymic macrophages were fate mapped, i. e. from YS origin (Fig. 3c). However, GFP^+ thymic macrophages decreased to just ~11% at E19.5, suggesting that YS progenitors establish the embryonic thymic macrophage pool but are quickly replaced by subsequent wave(s) of fetal liver monocytes or HSC-derived macrophages.

To pinpoint when do the HSC-derived progenitors enter the thymus, we devised two complementary experiments. First, we evaluated the contribution of circulating adult monocytes to thymic macrophages without the confounding effect of radiation damage on the thymus. We created shield chimeras by subjecting CD45.1 mice to a lethal dose of irradiation while protecting their upper body and the thymus with a 5 cm lead shield followed by reconstitution with CD45.2 bone marrow (Fig. 3d). While the donor-derived monocytes in the blood were, on average 20%, less than 2% of thymic macrophages were $CD45.2^+$ (Fig. 3e and f), suggesting a relatively minor (<10%) contribution of adult circulating monocytes to the thymic macrophage pool consistent with a previous report[37]. Second, we transplanted E15.5 embryonic thymuses expressing GFP ubiquitously under the control of the *ROSA26* locus (*ROSA26*^{GFP}) under the kidney capsule of adult mice and analyzed them six weeks later (Fig. 3g). By that time, >99% of thymocytes were derived from GFP^- host HSCs (Fig. 3h and i). As a positive control for donor-derived cells, we used the thymic epithelial cells. The vast majority of $EpCAM^+$ thymic epithelial cells (>90%) were still GFP^+. An identical proportion of thymic macrophages was also GFP^+. The results from our

transplantation experiments show that the progenitors of almost all thymic macrophages are of embryonic origin. Altogether our results suggest that resident thymic macrophages are derived from multiple waves of progenitors. Initially, the thymus is settled by YS-derived progenitors that contribute substantially to the thymic macrophage pool during the embryonic period. In parallel with them, YS-independent progenitors infiltrate the thymus before E15.5 and establish themselves as the dominant population before birth. Adult HSC-derived monocytes contribute relatively little to the pool of thymic resident macrophages in young adult mice.

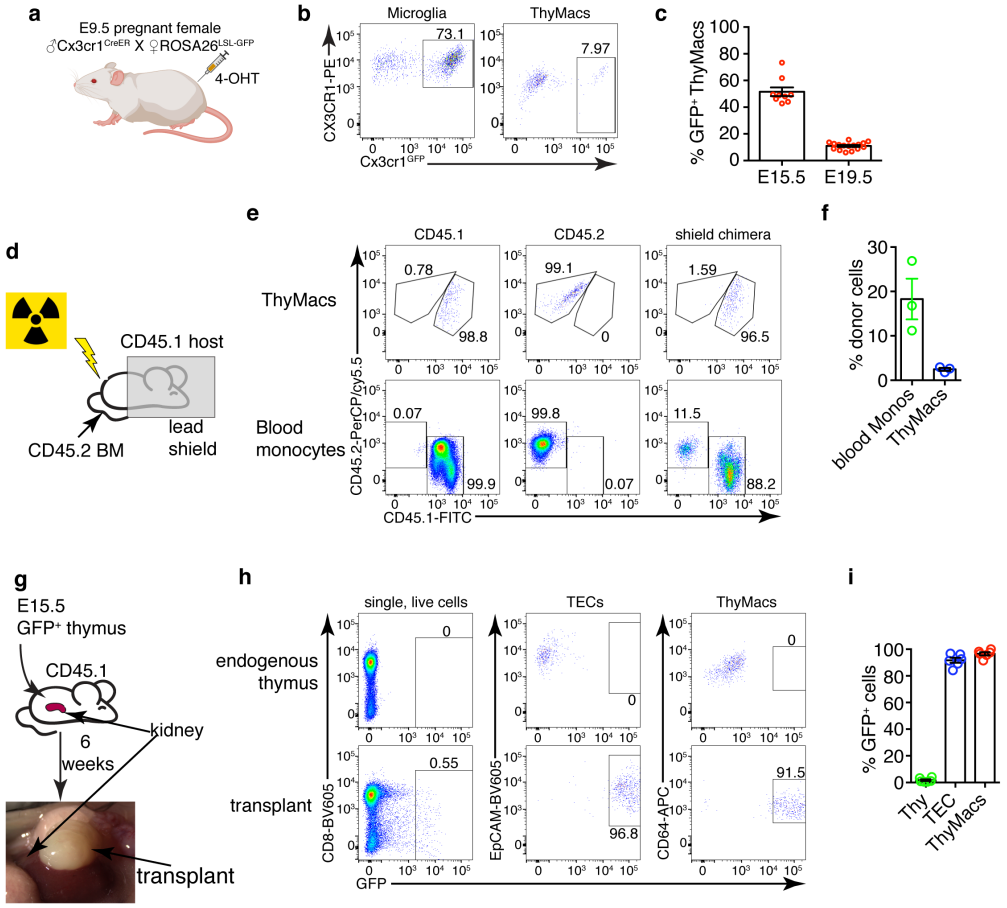

Figure 3. Yolk sac (YS)-derived and non-YS-derived embryonic progenitors sequentially contribute to the thymic macrophage pool. a Scheme of the YS-progenitor labeling experiments. E9.5 pregnant *ROSA26*$^{LSL\text{-}GFP}$ mice mated with *Cx3cr1*^{CreER} males were injected with 4-

hydroxytamoxifen (4-OHT) and sacrificed at E15.5 or E19.5. **b** Representative flow cytometry plots of the *Cx3cr1*^{GFP} expression in microglia (CD45$^+$CD11b$^+$ cells in the brain) and ThyMacs of the pups. **c** Frequencies of GFP$^+$ ThyMacs at E15.5 and E19.5 adjusted to the degree of labeling of microglia. **d** Scheme of the shield chimera experiments. Congenic CD45.1 mice were lethally irradiated with their upper body protected by a 5 cm thick lead shield and then injected with CD45.2$^+$ bone marrow. **e** Representative flow cytometric analysis of ThyMacs and CD115$^+$CD11b$^+$ blood monocytes for donor-derived (CD45.2$^+$) cells. Non-chimeric CD45.1 and CD45.2 samples serve as controls for the gating. **f** Frequencies of donor-derived ThyMacs and blood monocytes. **g** Scheme of the thymus transplantation experiments. **h** Representative flow cytometry plots of GFP expression in thymocytes (Thy), CD45$^-$EpCAM$^+$ thymic epithelial cells (TECs), and thymic macrophages (ThyMacs) six weeks after the transplantation. The host thymus (endogenous thymus) serves as a negative control. The percentages of GFP$^+$ cells are indicated in the plots. **i** Frequencies of GFP$^+$ cells in different cell populations in the transplanted thymus. Data in **c**, **f**, and **i** are mean±SEM with two litters, three, and five mice per group, respectively. The numbers in the flow cytometry plots are the percent of cells in the respective gates. Each dot is an individual mouse or embryo.

Thymic macrophages can proliferate in situ

The fact that macrophages can persist for many weeks in the thymus without constant replacement from blood monocytes suggests that they can divide in situ. Staining for the proliferation marker Ki-67 revealed that ~4% of

the cells expressed this marker compared to an isotype control (Fig. 4a and b). To obtain further proof that thymic macrophages are proliferative, we tested the incorporation of the nucleotide analog 5-Ethynyl-2'-deoxyuridine (EdU). Short-term EdU labeling experiments unexpectedly revealed that thymic macrophages become EdU^+ with faster kinetics than thymocytes (Fig. 4c). The most likely explanation for this puzzling result is that some of the thymic macrophages have engulfed apoptotic thymocytes that have recently divided and incorporated EdU. Thus, EdU could have accumulated in these macrophages through phagocytosis and not through cell division. To circumvent this caveat, we designed a pulse-chase experiment (Fig. 4d). Mice were injected daily with EdU for 21 days so that all cells that proliferate in that period would incorporate the label. The vast majority of thymocytes and thymic macrophages became EdU^+ at d. 21 (Fig. 4e). After 21 more days of "chase period", only ~0.2% of thymocytes had retained the EdU label, consistent with the existence of a very small population of long-term resident thymocytes consisting mainly of regulatory T cells and NKT cells[54] (Fig. 4e and f). However, ~5% of the thymic macrophages were EdU^+, suggesting they divided during the labeling period. Finally, we sorted thymic macrophages and subjected them to cell cycle analysis. Although almost all thymic macrophages were in G0/G1 phase, a small population of ~3% was in G2/M phase of the cell cycle (Fig. 4g and h). Collectively, three independent approaches documented that 3-5% of thymic macrophages are actively dividing under homeostatic conditions within the thymus. These findings can explain the long-term maintenance of these cells within the organ without a constant influx of progenitors.

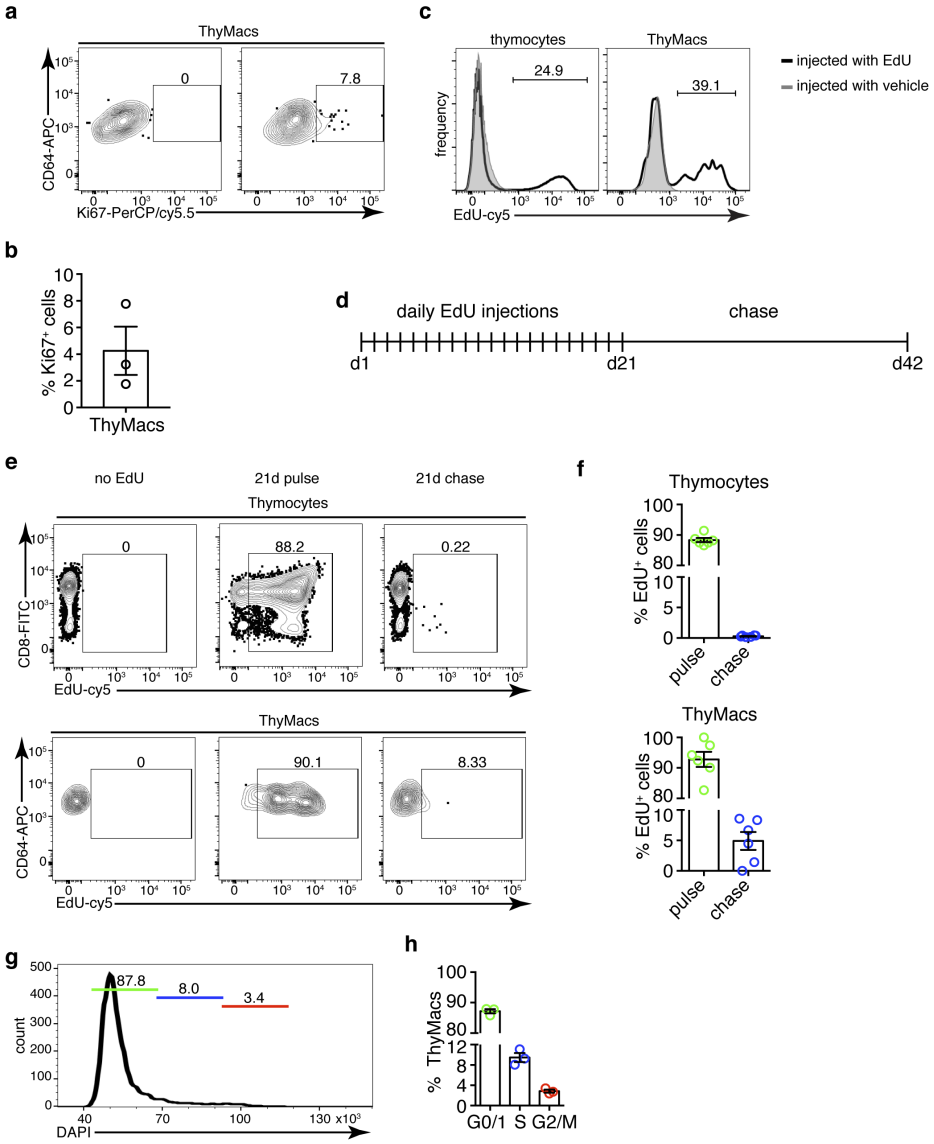

Figure 4. Thymic macrophages exhibit a low degree of proliferation. a Example flow cytometry plots of Ki67 staining of thymic macrophages (ThyMacs). **b** Frequency of Ki67⁺ thymic macrophages. **c** Example flow cytometry plots of the EdU accumulation in thymocytes and thymic macrophages 2 hours after 1 mg EdU i.p. or vehicle injection. The numbers inside flow plots are the percentage of EdU⁺ cells from mice injected with EdU. Data are representative of three independent experiments. **d** Scheme of EdU pulse/chase experiment: mice were injected daily with 1 mg EdU i.p for 21 days and then rested for 21 more days. **e** Example flow cytometry plots of

EdU staining of thymocytes (upper row) and ThyMacs (lower row). **f** Frequencies of EdU$^+$ cells among thymocytes (top graph) and ThyMacs (bottom graph). **g** Example flow cytometry plot of cell cycle analysis of FACS sorted ThyMacs. **h** Frequencies of ThyMacs in different stages of the cell cycle. The numbers in the flow cytometry plots are the percent of cells in the respective gates. Data are mean±SEM from three mice (**b** and **h**) or 6-7 individual mice (**f**). Each dot is an individual mouse.

Expression of *Timd4* and *Cx3cr1 can distinguish* two populations of thymic macrophages

To determine if thymic macrophages are heterogeneous, we turned to our scRNA-Seq data. Once we zoomed onto *Mafb* expressing cells, we could distinguish three separate populations: 1) monocytes that expressed high levels of *Ly6c2* and *Itgam* (CD11b) but did not express *Mertk*; 2) *Timd4*$^+$ (encoding TIM4) macrophages that also expressed high levels of *Spic* and *Slc40a1*, but low levels of *Cx3cr1*; 3) *Cx3cr1*$^+$ macrophages that expressed low levels of *Timd4*, *Spic*, and *Slc40a1* (Fig. 5a and b). Both macrophages and monocytes expressed *Fcgr1* (CD64). A minority of macrophages expressed high levels of *Mki67*, indicating that they might be proliferating, corroborating our earlier data. Interestingly, most of the *Mki67* expressing macrophages belonged to the *Cx3cr1*$^+$ population.

We confirmed the results from scRNA-Seq by flow cytometry. We could identify discrete TIM4$^+$*Cx3cr1*$^{GFP-}$ and TIM4$^-$*Cx3cr1*$^{GFP+}$ macrophages (Fig. 5c). There was even TIM4$^+$*Cx3cr1*$^{GFP+}$ intermediate population that could not be distinguished in the scRNA-Seq dataset, likely because of the lack of

434 statistical power. To determine the localization of the two distinct macrophage
435 populations, we stained thymic sections from *Cx3cr1*^{GFP} mice with an antibody
436 to MerTK. The *Cx3cr1*$^{GFP-}$ MerTK^{+} cells correspond to *Timd4*$^{+}$ macrophages,
437 while the *Cx3cr1*$^{GFP+}$MerTK^{+} cells would be the *Cx3cr1*$^{GFP+}$ macrophages.
438 Strikingly, the two macrophage populations showed distinct localization.
439 *Timd4*$^{+}$ macrophages were located in the cortex, while the *Cx3cr1*$^{GFP+}$
440 macrophages resided in the medulla and the cortico-medullary junction (Fig.
441 5d).
442 To better understand the differences between the two populations of thymic
443 macrophages, we looked for differentially expressed genes. We included the
444 thymic monocytes in the comparison, as these cells clustered the closest to
445 macrophages. *Timd4*$^{+}$ macrophages expressed the highest levels of the
446 transcription factors *Spic*, *Maf*, and *Nr1h3*; the receptors for apoptotic cells
447 *Axl*, *Mertk*, and *Timd4*; and many Slc transporters such as *Slc40a1*, *Slc1a3*,
448 *Slco2b1*, *Slc11a1*, and *Slc7a7* (Fig. 5e and Table S2). *Cx3cr1*$^{+}$ macrophages
449 expressed high levels of the transcription factor *Runx3*; a distinct set of
450 phosphatidylserine receptors such as *Stab1*, *Anxa5*, and *Anxa3*; many
451 degradative enzymes such as *Mmp2*, *Mmp14*, *Dnase1l3*, *Acp5*, *Lyz2*, *Ctsz*,
452 *Ctss*, *Ctsd*, *Ctsl*; cytokines such as *Pdgfa*, *Cxcl16*, and *Ccl12*; and molecules
453 involved in MHC1 antigen presentation such as *B2m*, *H2-M2*, *H2-K1*, *H2-Q7*.
454 Thymic monocytes were characterized by differential expression of the typical
455 monocyte genes *Ly6c2*, *Ccr2*, and *S100a4*, and genes involved in MHC2
456 antigen presentation such as *Ciita*, *H2-DMb1*, *H2-Ab1*, and *Cd74*.
457

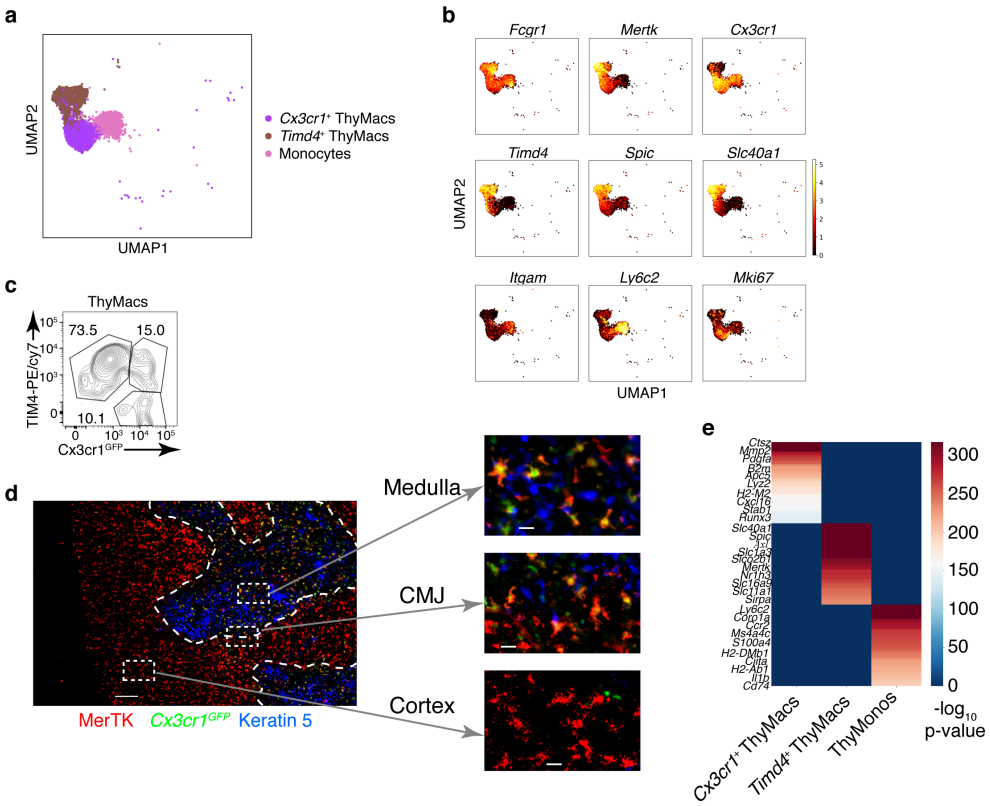

458 Figure 5: **Two populations of macrophages with distinct localization**
459 **exist in the thymus. a** UMAP clusters from Fig. S2 with high expression of
460 the transcription factor *Mafb* fall into three groups: monocytes, *Timd4*$^{+}$
461 macrophages, and *Cx3cr1*$^{+}$ macrophages. **b** Expression of the indicated
462 genes in the three *Mafb*-positive clusters. **c** A flow cytometry plot of *Cx3cr1*^{GFP}
463 and TIM4 expression in ThyMacs. The plot is representative of >10 individual
464 experiments. The numbers inside the plot are the percentages of the cell
465 populations in the respective gates. **d** Immunofluorescent staining of the
466 thymus of *Cx3cr1*^{GFP} mouse stained with MerTK (a marker for all
467 macrophages) and Keratin 5 (a marker for medulla). The scale bar is 150 μm.
468 Areas in the cortex, medulla, and the cortico-medullary junction (CMJ)
469 represented by the dashed boxes are enlarged below to show the co-
470 localization of *Cx3cr11*^{GFP} and MerTK signal in CMJ and medulla, but not in
471 cortex. The scale bars in the images below are 20 μm. The images are

representative of three individual mice. **e** Differentially expressed genes among *Timd4*$^+$ thymic macrophages, *Cx3cr1*$^+$ thymic macrophages, and thymic monocytes. The negative $\log_{10}$ p-values for the genes expressed in each cluster were calculated as described in the Materials and Methods, and the top 50 differentially expressed genes were plotted in the figure. Ten of these genes are listed on the left.

Cx3cr1$^+$ cells give rise to *Timd4*$^+$ cells during embryonic development

To determine if the two populations of thymic macrophages are related, we first analyzed the kinetics of their appearance during embryonic development. At the earliest time point (E14.5), all thymic macrophages were *Cx3cr1*$^+$, and only ~20% of them were also TIM4$^+$ (Fig. 6a and b). The proportion of TIM4$^+$ cells increased at E17.5, and TIM4$^+$*Cx3cr1*$^-$ cells started to appear. In the neonatal period, almost all macrophages were TIM4$^+$, and very few remained TIM4$^-$. The proportion of TIM4$^-$ cells increased in 6 weeks old mice, but TIM4$^+$ macrophages remained the dominant population. These kinetics (Fig. 6c) are consistent with *Timd4*$^+$ macrophages developing from *Cx3cr1*$^+$ cells before birth. Another plausible scenario is that distinct progenitors give rise to different thymic macrophages populations (e.g., YS-progenitors give rise to *Cx3cr1*$^+$*Timd4*$^-$ and HSC-derived progenitors develop into *Timd4*$^+$ macrophages). To test the latter hypothesis, we re-visited the fate mapping of YS progenitors results (Fig. 3a). Although a larger part (~60% at E15.5) of *Cx3cr1*$^+$TIM4$^-$ cells were derived from YS progenitors (Fig. 6d), a substantial proportion (~40% at E15.5) of YS-derived TIM4$^+$ macrophages could clearly be identified at both E15.5 and E19.5, suggesting that YS progenitors can

497 give rise to both *Cx3cr1*$^{+}$ and *Timd4*$^{+}$ cells. Extrapolating from the data, the
498 non-YS-derived progenitors (GFP^{-} cells) can also give rise to both *Timd4*$^{-}$ and
499 *Timd4*$^{+}$ cells. Thus, the simplest explanation for our findings is that *Timd4*$^{+}$
500 cells develop from *Cx3cr1*$^{+}$ cells during embryonic development. This
501 transition is complete in the first week after birth as there were essentially no
502 *Cx3cr1*$^{+}$ thymic macrophages remaining at d.7 (Fig. 6a and b).

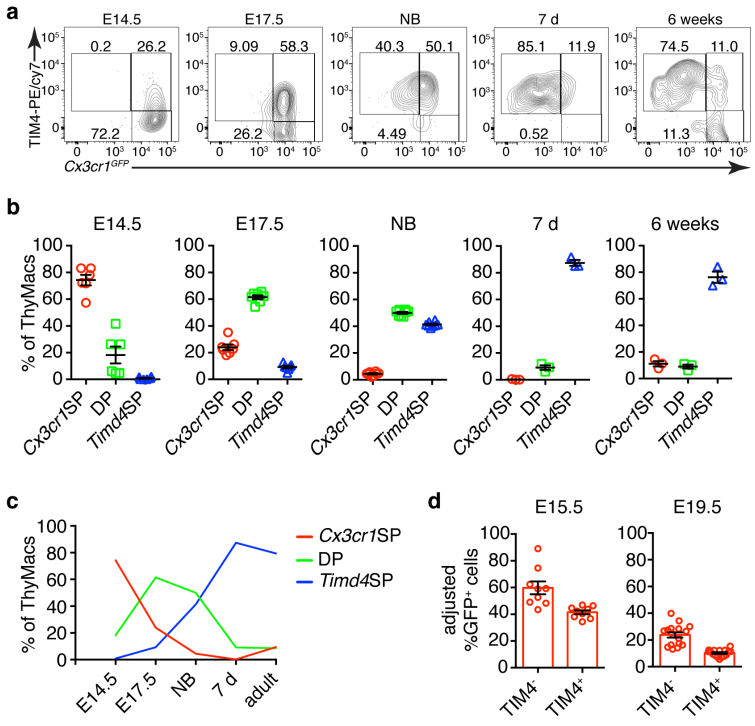

503

504 **Figure 6. *Timd4*$^{+}$ thymic macrophages are derived from *Cx3cr1*$^{+}$ cells**
505 **during embryonic development. a** Example flow cytometry plots for the
506 expression of *Cx3cr1*^{GFP} and TIM4 on thymic macrophages at different times
507 during embryonic development (E14.5, E17.5), immediately after birth, at 7
508 days, and 6 weeks of age. **b** Frequencies of *Timd4*$^{+}$*Cx3cr1*$^{-}$ (*Timd4* single-
509 positive or *Timd4*SP), *Timd4*$^{+}$*Cx3cr1*$^{+}$(double-positive or DP), and
510 *Cx3cr1*$^{+}$*Timd4*$^{-}$ (*Cx3cr1* single-positive or *Cx3cr1*SP) thymic macrophages at
511 the indicated time points. **c** Kinetics of the changes in different subpopulations
512 of thymic macrophages from E14.5 to 6 weeks. **d** Frequencies at E15.5 and

E19.5 of GFP-labeled cells among *TIM4*$^{+}$ or *TIM4*$^{-}$ cells in *Cx3cr1*^{CreER} X *ROSA26*$^{LSL\text{-}GFP}$ embryos treated with 4-OHT at E9.5. Data is from at least two independent experiments for each panel. Each symbol is an individual mouse or embryo.

Timd4^{+} thymic macrophages self-maintain, while _Cx3cr1_$^{+}$ cells slowly accumulate with age

To understand how are the resident thymic macrophage populations maintained during adult life, we induced recombination in *Cx3cr1*^{CreER} X *ROSA26*$^{LSL\text{-}GFP}$ mice during the neonatal period (Fig. 7a) or at 6 weeks of age (Fig. 7c) and compared the proportion of GFP^{+} cells 3 and 42 days after labeling. The extent of labeling of *Timd4*$^{+}$ thymic macrophages did not change within these 6 weeks, no matter whether the mice were treated with Tamoxifen in the first week after birth or at 6 weeks (Fig. 7b and d), suggesting steady-state maintenance and absence of a significant influx from unlabeled cells (e.g., monocytes). In contrast, the proportion of labeled *Timd4*$^{-}$ thymic macrophages decreased significantly 6 weeks after Tamoxifen injection in both neonatal and adult mice, suggesting that this population was being diluted by unlabeled cells. To further substantiate these findings, we examined older WT mice and found out that the proportions of *Timd4*$^{-}$ thymic macrophages increased with age, and in mice >8 months old, they accounted for ~70% of all macrophages in the organ (Fig. 7e). Thus, we conclude that *Timd4*$^{+}$ macrophages can maintain themselves for long periods in the cortex of the thymus, Since the first week of life, *Cx3cr1*$^{+}$ cells are slowly being recruited to the medulla and cortico-medullary junction, and in aging mice

538 form the predominant phagocytic population in the organ.

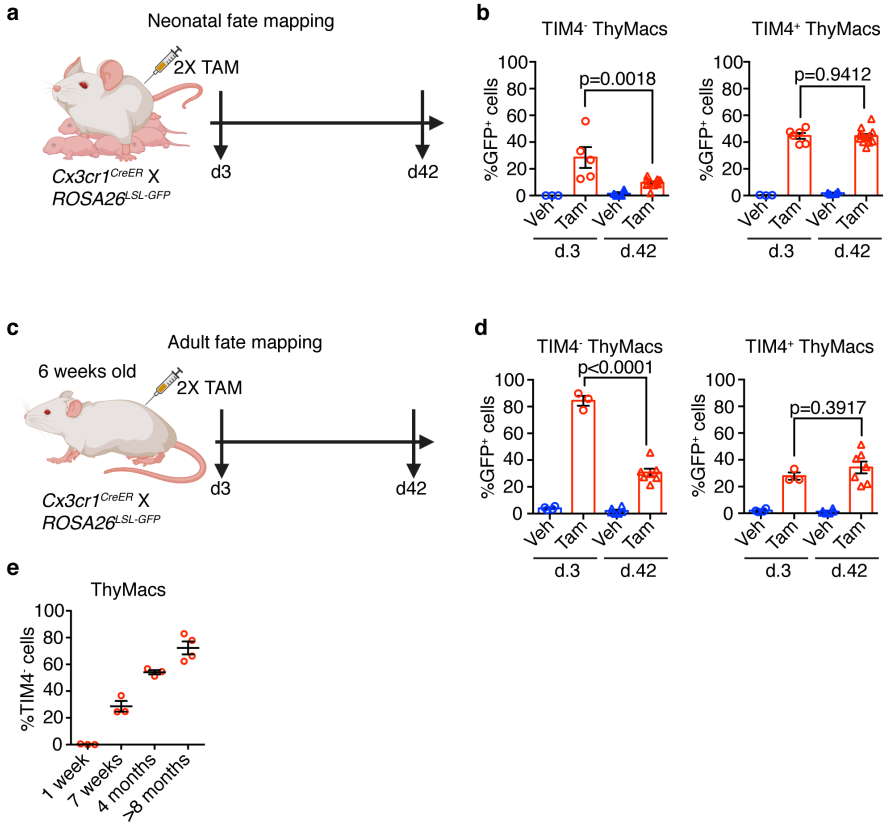

539

540 **Figure 7. *Timd4*⁺ thymic macrophages self-maintain during adult life,**

541 **while *Cx3cr1*⁺ cells slowly accumulate with age. a** Scheme of the neonatal

542 fate mapping: A nursing dam was injected twice with Tamoxifen (Tam) or

543 vehicle (Veh) in the first week after giving birth to *Cx3cr1*^{CreER} X *ROSA26*$^{LSL-}$

544 ^{GFP} pups. Three or 42 days after the last injection, the pups were sacrificed,

545 and the degree of labeling of *Timd4*⁺ and *Timd4*⁻ thymic macrophages was

546 examined by flow cytometry. **b** Frequencies of GFP⁺ *Timd4*⁺ or *Timd4*⁻ thymic

547 macrophages from neonatally fate mapped mice after 3 and 42 days. Vehicle

548 injected nursing dam litters (Veh) served as a control for non-specific labeling.

549 **c** Scheme of the adult fate mapping: Six weeks old *Cx3cr1*^{CreER} X *ROSA26*$^{LSL-}$

550 ^{GFP} mice were injected twice with Tamoxifen (Tam) or vehicle (Veh). Three or

551 42 days after the last injection, the mice were sacrificed, and the degree of

552 labeling of *Timd4*⁺ and *Timd4*⁻ thymic macrophages was examined by flow

553 cytometry. **d** Frequencies of GFP$^+$ *Timd4*$^+$ or *Timd4*$^-$ thymic macrophages
554 from adult fate mapped mice after 3 and 42 days. **e** Frequencies of TIM4$^-$
555 thymic macrophages at different ages. The data is mean±SEM from 2
556 independent experiments (**b**) or at least 3 individual mice per time point (**d** and
557 **e**). Each symbol is an individual mouse. Statistical significance was
558 determined with unpaired Student's t-test.
559
560 **Discussion**
561 Here, we have described the phenotype, transcriptional profile, localization,
562 diversity, ontogeny, and maintenance of macrophages in the thymus. These
563 cells express the typical macrophage markers CD64, MerTK, and F4/80 and
564 are transcriptionally most similar to splenic red pulp macrophages and liver
565 Kupffer cells. However, they have a unique expression profile dominated by
566 genes involved in antigen presentation and lysosomal degradation. We found
567 that thymic macrophages consist of two populations with distinct localization.
568 *Timd4*$^+$ macrophages occupied the cortex, while *Cx3cr1*$^+$ cells were located in
569 the medulla and the cortico-medullary junction. While YS-derived
570 macrophages dominated the early stages of thymus development, they were
571 quickly replaced by non-YS embryonic progenitors that gave rise to the
572 *Timd4*$^+$ thymic macrophages that could proliferate and self-maintain. *Cx3cr1*$^+$
573 macrophages started slowly accumulating after birth and in old mice became
574 the most abundant population.
575 Altogether our data depict thymic macrophages as typical tissue-resident
576 macrophages with origin from multiple hematopoietic waves, ability to self-
577 maintain, and expression of the core macrophage-specific genes. They were

most similar transcriptionally to splenic red pulp macrophages and Kupffer cells, which is not surprising considering that they all specialize in efferocytosis and have efficient lysosomal degradation machinery. These three populations also shared expression of the transcription factor *Spic* that is induced by heme released following red blood cells phagocytosis[52]. However, the thymus is not known as a place for erythrocyte degradation. Thus the mechanism for *Spic* up-regulation in thymic macrophages is unclear.

The unique features of thymic macrophages include high expression of genes involved in the IFN-I pathway, antigen presentation, and lysosomal degradation. The up-regulation of IFN-I-stimulated genes such as *Stat1*, *Stat2*, *Irf7*, and *Irf8* can be explained by the constitutive secretion of IFN-I by thymic epithelial cells[55,56]. The purpose of IFN-I expression in the thymus in the absence of a viral infection is unclear. Still one possibility is that it mediates negative selection to IFN-dependent genes as part of central tolerance.

Thymic macrophages highly express molecules involved in antigen presentation, including MHC1 and MHC2, although the latter is expressed at lower levels than in cDCs. Thus, they have the potential to present antigens for both negative selection and agonist selection. These two activities have traditionally been assigned solely to cDCs[57]. However, recent evidence suggests that negative selection is most efficient when the cell that presents the antigen to auto-reactive thymocytes is also the one that phagocytoses it[58]. So, macrophages participation in thymocyte selection needs to be re-evaluated with optimized isolation procedures and specific genetic tools.

The extraordinary ability of thymic macrophages to engulf and degrade apoptotic thymocytes has been appreciated for a long time[31], and our RNA-Seq data provides additional supporting evidence for this function by highlighting the up-regulation of pathways involved in lysosomal degradation. An interesting topic for future research would be to understand how the metabolites derived from apoptotic cells are returned to the microenvironment to support the proliferation of immature thymocytes. A *SoLute Carrier* (*Slc*) genes-based program has been described in vitro[59], but its relevance to tissue-resident macrophages remains to be determined. Altogether, our study demonstrates that thymic macrophages are a unique subset of tissue-resident macrophages and support the idea that resident macrophage phenotype is determined by the combination of ontogeny, microenvironment, and other factors[60].

Together with the study by Tacke et al., our work builds the following model for thymic macrophage origin[37]: Thymic macrophages develop in three distinct waves: YS-derived progenitors dominate the early stages of thymus development but are replaced before birth by a second wave of YS-independent embryonic progenitors that forms the bulk of thymic macrophages after birth and can self-maintain into adulthood. With age, there is a slow and steady influx of *Timd4*$^{-}$*Cx3cr1*$^{+}$ macrophage precursors that occupy the medulla and cortico-medullary junction, becoming the major phagocytic population in the thymus of older mice (>8 months). The second wave of YS-independent macrophages is most likely the progeny of embryonic HSCs based on *Flt3*^{Cre} fate mapping that showed that >80% of thymic macrophages in adult mice are descendants of HSCs[37]. Whether

627 HSC-independent fetal liver monocytes contribute to thymic macrophages and
628 to what extend awaits the creation of models that can specifically target this
629 population of progenitors. Recruitment of circulating monocytes to the resident
630 macrophage pool in the thymus has been ruled out previously by parabiosis
631 and *Ccr2*$^{-/-}$ mice[37]. Our shield chimera experiments have arrived at similar
632 conclusions. However, the relatively short duration of these experiments and
633 their focus on the bulk thymic macrophages have prevented the recognition of
634 the gradual accumulation of *Timd4*$^{-}$ macrophages. Once we zoomed in on this
635 minor cell population in young mice, the fate mapping clearly showed an influx
636 of unlabeled progenitors. Whether the progenitors of *Timd4*$^{-}$ macrophages
637 are monocytes remains to be formally demonstrated. However, in all
638 macrophage populations exhibiting replacement in adults examined to date,
639 monocytes have been singled out as the source[12,19,22,24,25,30]. An
640 alternative possibility involves thymocyte progenitors that under certain
641 circumstances have been shown to differentiate into macrophages and
642 granulocytes in the thymus[42,43]. However, if this occurs in unmanipulated
643 mice at a steady-state remains unclear.
644 The strict spatial segregation of the two macrophage populations in the
645 thymus implies that they might have distinct functions. *Timd4*$^{+}$ cells are
646 restricted to the cortex and are particularly abundant in the deeper cortex,
647 close to the medulla. Both positive and negative selection of thymocytes occur
648 there, so we speculate that *Timd4*$^{+}$ macrophages might be specialized in
649 efferocytosis of CD4^{+}CD8^{+} (double-positive) thymocytes that cannot interact
650 with cortical thymic epithelial cells and die by neglect or are auto-reactive and
651 undergo clonal deletion in the cortex[61]. On the other hand, *Cx3cr1*$^{+}$

macrophages accumulate in the medulla; the thymic region specialized in negative selection to tissue-restricted antigens (TRA). They might contribute to the process in several ways: 1) by carrying TRAs from blood and peripheral organs. A similar process has been described for cDC2 (SIRPα^+ DCs)[62]. In fact, *Cx3cr1*$^+$ thymic macrophages could have contributed to this role because they were not distinguished from cDC2 in this study. 2) By capturing TRAs from *Aire*$^+$ medullary thymic epithelial cells and presenting them to auto-reactive thymocytes as shown for DCs[63-65]. 3) By phagocytosing apoptotic TRA-specific medullary thymocytes, a process we have observed before[58]. The exact involvement of thymic macrophages in the selection events in the thymus remains to be determined.

The accumulation of the *Cx3cr1*$^+$ cells in older mice has clear implications for thymus aging. One key feature of thymus involution is the accumulation of extracellular matrix produced by fibroblasts and the emergence of white adipocytes[66]. The *Cx3cr1*$^+$ subset is the predominant producer of the growth factor PDGFα that is required for the maintenance of adipocyte stem cells and can stimulate tissue fibrosis[67,68]. The gradual accumulation of *Cx3cr1*$^+$ macrophages could increase the availability PDGFα in the aging thymus stimulating extracellular matrix production and differentiation of precursors into adipocytes. This model predicts that limiting the influx of *Cx3cr1*$^+$ macrophage precursors could delay thymus involution.

Recent work described a novel phagocytic and antigen-presenting cell type in the thymus called monocyte-derived DCs[65]. The phenotype of these cells overlaps with the CD64$^+$F4/80^{lo}CD11b$^+$ cells in our study. However, we favor the classification of these cells as monocytes based on their expression of

Mafb, CD64, and Ly6C (Fig. 5b) and lack of expression of the defining DC transcription factor *Zbtb46* (Fig. S2c)[69]. As monocytes can differentiate into cDC2, particularly in the context of inflammation[70], the precise identity and the relationship of this population to thymic cDC2 remain to be established.

In the past several years, scRNA-Seq has come to the forefront of biologists' efforts to disentangle the cellular diversity of tissues. Several comprehensive studies have included samples from mouse or human thymus[71-73]. However, in these studies, too few thymic macrophages were sampled to give meaningful clustering results. Efforts specifically targeting the thymus have provided considerably more information[74,75], but macrophage diversity was still not recognized. Characterization of rare populations such as thymic macrophages (~0.1% of all cells in the thymus) requires optimized enzymatic digestion procedures and enrichment strategies, as has been demonstrated already for thymic epithelial cells[76,77]. Our scRNA-Seq dataset provides a rich resource for the unbiased characterization of myeloid cells in the thymus and will greatly aid in the understanding of the myeloid landscape of the thymus.

In summary, our work comprehensively characterizes macrophages in the thymus and paves the way for exploration of their functions.

Materials and methods

Mice

C57BL/6Narl (CD45.2) mice were purchased from the National Laboratory Animal Center, Taipei, Taiwan. MAFIA (MAcrophage Fas-Induced Apoptosis) [78], *Cx3cr1*^{GFP} [79], *Spic*^{GFP} [52], *Cx3cr1*^{CreER} [53], and *B6.SJL-Ptprca*

Pepcb/BoyJ (CD45.1) mice were purchased from the Jackson Laboratories. *Cd11c*^{YFP} [80] and *Lyz2*^{GFP} [81] mice have been described. Mice ubiquitously expressing GFP from the *ROSA26* locus were generated by breeding *Pdgfra*^{Cre} [82] and *ROSA26*$^{LSL\text{-}ZsGreen}$ (also known as *ROSA26*$^{LSL\text{-}GFP}$ or Ai6) mice[83] (both from the Jackson Laboratories). A mouse from this cross was identified, in which the STOP cassette was deleted in the germline. It was designated *ROSA26*^{GFP} and subsequently bred to C57BL/6 mice. All mice were used at 4-10 weeks of age unless otherwise specified. Mice were bred and maintained under specific pathogen-free conditions at the animal facility of National Yang-Ming University. All experimental procedures were approved by the Institutional Animal Care and Use Committee (IACUC) of National Yang-Ming University.

Treatment with 5-Ethynyl-2'-deoxyuridine (EdU)

Mice were i.p. injected with 1 mg EdU (Carbosynth) dissolved in PBS daily for 21 days and then rested for 21 more days. Cells from the thymus were harvested on day 21 or 42. In some experiments, the mice were sacrificed 2 hours after the first EdU injection.

Shield chimera generation

CD45.1 mice were anesthetized by i.p. injection of 120 μg/g body weight Ketamine hydrochloride (Toronto Research Chemicals) and 12 μg/g body weight Xylazine hydrochloride (Sigma). Anesthetized mice were taped to a 5 cm thick lead block so that the lead block covered the head and the chest down to the bottom of the rib cage. Then, they were irradiated with a lethal

dose (1000 rad) from a ^{137}Cs source (Minishot II, AXR) so that only their abdomen and hind legs were exposed. After recovery from anesthesia, the mice were transfused i.v. with 10^7 bone marrow cells from a congenic (CD45.2) donor. Then, they were given Trimerin (0.5 mg/mL Sulfadiazine + 0.1 mg/mL Trimethoprim, China Chemical and Pharmaceutical Co., Tainan, Taiwan) in the drinking water for the first two weeks after the irradiation and analyzed after six weeks.

Cell isolation from thymus, blood, and peritoneal cavity

Thymocytes were obtained by mechanical disruption of the thymus with a syringe plunger. For myeloid cell isolation, mouse thymuses were cut into small pieces and digested with 0.2 mg/mL DNase I (Roche) and 0.2 mg/mL collagenase P (Roche) in complete DMEM for 20 min at 37˚C with frequent agitation. 1.6 mg/mL Dispase I (ThermoFisher) was added to the enzymatic mixture for thymic epithelial cell isolation. In some experiments, thymic myeloid cells and thymic epithelial cells were enriched by 57% Percoll PLUS (GE Healthcare) discontinuous gradient centrifugation at 4˚C, 1800 rpm, for 20 min without brake. Cells at the interface were collected and washed with PBS to remove residual silica particles. Then the cells were resuspended in PBS with 0.5% BSA (HM Biological), filtered through a 70 μm filter, and kept on ice.

Blood was isolated by cardiac puncture of sacrificed mice and immediately diluted with PBS. After centrifugation, the cell suspensions were treated with ammonium chloride-potassium lysis buffer for 3 min on ice once or twice.

752 Peritoneal cavity cells were obtained by lavage with 5 mL PBS + 2 mM EDTA
753 (Merck). Following gentle massage, the cavity was opened with an abdominal
754 incision, and lavage fluid was collected.
755
756 **Flow cytometry**
757 Single-cell suspensions (0.5 – 2X10^6 cells) from thymus, blood, or
758 peritoneal cavity were blocked with supernatant from 2.4G2 hybridoma (a kind
759 gift by Dr. Fang Liao, Academia Sinica, Taipei, Taiwan) and stained with
760 fluorochrome- or biotin-labeled antibodies for 20 min on ice in PBS + 0.5%
761 BSA + 2 mM EDTA + 0.1% NaN_3 (FACS buffer). The following antibodies
762 were used: CD11b (clone M1/70), MHC2 (M5/114.15.2), CD11c (N418),
763 F4/80 (BM8), CD115 (AFS98), SIRPα (P84), CD45 (30-F11), NK1.1 (PK136),
764 TIM4 (RMT4-54), Gr-1 (RB6-8C5), CD64 (X54-5/7.1), Siglec H (551), Ly6C
765 (HK1.4), CD3ε (145-2C11), CD8α (53-6.7), CD19 (6D5), B220 (RA3-6B2),
766 CD4 (GK1.5), CD51 (RMV-7), CD45.1 (A20), CD45.2 (104), CX3CR1
767 (SA011F11), and EpCAM (G8.8) from BioLegend; Axl (MAXL8DS), MerTK
768 (DS5MMER), and Ki67 (SolA15) were from eBioscience; Siglec F (E50-2440),
769 CD90.2 (30-H12), and CD11c (HL3) were from BD Biosciences. Cells were
770 washed, and if necessary, incubated for 20 more min with fluorochrome-
771 labeled Streptavidin: Streptavidin-AF647 (Jackson Immunoresearch) or
772 Streptavidin-APC/cy7, Streptavidin-BV421, Streptavidin-BV605 (BioLegend).
773 After the last wash, the cells were resuspended in FACS buffer containing
774 DAPI (BioLegend), Propidium Iodide (Sigma), or DRAQ7 (BioLegend) and
775 analyzed immediately on an LSR Fortessa flow cytometer running Diva 8

776 software (BD Biosciences). Typically, 500,000 cells were collected from
777 thymus samples. Data were analyzed using FlowJo software (TreeStar).
778
779 For intracellular staining, after surface antibody staining, the cells were
780 labeled with Zombie Aqua (BioLegend) for 30 min in ice. Then, the cells were
781 fixed with 2% paraformaldehyde (Electron Microscope Sciences) in PBS for
782 20 min on ice, permeabilized with either 0.5% Triton-X 100 (Sigma) for 20 min
783 on ice, or with Foxp3 staining kit (eBioscience) according to the protocol
784 provided by the manufacturer, and stained with antibodies for intracellular
785 markers for 40-60 min on ice.
786
787 For cell cycle analysis, 1-5X10^5 sorted thymic macrophages were fixed with
788 70% ethanol for 2 h on ice. The cells were spun down at 1800 rpm for 20 min
789 at 4˚C, washed with PBS, and stained with 1 μg/ml DAPI (BioLegend) for 30
790 min at room temperature in the dark.
791
792 For EdU staining, after surface marker and Zombie Aqua staining, cells
793 were fixed with 2% paraformaldehyde in PBS for 20 min on ice and
794 permeabilized with 0.5% Triton X-100 in PBS at room temperature for 20 min.
795 EdU was detected by adding an equal volume of 2X Click reaction buffer
796 consisting of 200 mM Tris, 200 mM ascorbic acid (Acros), 8 mM $CuSO_4$
797 (Acros), 8 μM Cy5-azide (Lumiprobe) to the permeabilized cells resuspended
798 in 0.5% Triton X-100 in PBS and incubation at room temperature for 30 min.
799 Cells were washed twice with 0.5% Triton X-100 in PBS and analyzed on a
800 flow cytometer.

Cell sorting

The sorting of thymic macrophages was done following the IMMGEN guidelines. Briefly, the thymuses of 3 male C57BL/6Narl mice were harvested in ice-cold staining buffer containing phenol red-free DMEM (Gibco) with 10 mM HEPES (Sigma), 0.1% NaN_3, and 2% FBS (Gibco). Single-cell suspensions were prepared as described in the Flow cytometry section. Percoll PLUS was used to enrich mononuclear cells. The cells were resuspended at 10^8/mL in staining buffer and labeled with appropriate antibodies for 15 min in ice. To sort thymic macrophages, the cells were first labeled with biotinylated antibodies to lineage markers (Lin) – CD3, CD8, Gr1, B220. After washing, the cells were stained with antibodies to CD11b, F4/80, CD45, CD64, and Streptavidin-APC/cy7 for 15 min in ice. For sorting thymus $XCR1^+$ and $SIRP\alpha^+$ cDCs, antibodies to XCR1, SIRPα, CD11c, MHC2, CD64, and F4/80 were used. For sorting peritoneal cavity macrophages, antibodies to ICAM2 and F4/80 were used. Immediately before sorting, the dead cells were excluded with DRAQ7 or PI. For RNA Sequencing experiments, the cells were double-sorted on FACS Melody, or Aria cell sorters (BD Biosciences) and 1000 cells were directly deposited in TCL buffer (Qiagen), frozen in dry ice and sent to IMMGEN for RNA sequencing. Four biological replicates were prepared. For cytospin and cell cycle analysis, 1-5X10^5 cells sorted on FACS Melody were collected in staining buffer.

Cytospin

Sorted cells were mounted on Superfrost PLUS slides (Thermo Scientific) using a Cytospin centrifuge (Cytospin 3, Shandon) for 5 min at 500 rpm. Cells were fixed with 2% paraformaldehyde for 10 min at room temperature and stained with the Hemacolor Rapid Staining Kit (Merck Millipore). Images were collected on BX61 upright microscope (Olympus) using 100X objective with immersion oil and captured with a CCD camera. Images were then analyzed and processed with ImageJ (NIH) and Adobe Photoshop 5.5 (Adobe).

RNA sequencing analysis

RNA sequencing was done at IMMGEN using Smart-seq2 protocol[84,85] on a NextSeq500 sequencer (Illumina). Following sequencing, raw reads were aligned with STAR to the mouse genome assembly mm10 and assigned to specific genes using the GENCODE vM12 annotation. Gene expression was normalized by DESeq2[86] and visualized by Morpheus (https://software.broadinstitute.org/morpheus). Hierarchical clustering was done with Cluster 3.0 and visualized with Java TreeView. Only genes with SD>20 were used (10602 genes). The metric used was Pearson correlation (uncentered), and the clustering method was average linking. Gene expression of mouse transcription factors[87] was visualized in MultiplotStudio of GenePattern[88]. GO enrichment was calculated and visualized in R by using clusterProfiler[89].

Timed pregnancies and embryonic thymus analysis

To set up timed pregnancies, each male mouse (*Cx3cr1*$^{CreER/CreER}$, *Cx3cr1*$^{GFP/GFP}$ or C57BL/6) and female mouse (*ROSA26*$^{LSL\text{-}GFP/LSL\text{-}GFP}$ or

C57BL/6) were housed together in the same cage for one night and separated on the next day, which we defined as embryonic day 0.5 (E0.5). Female mice were assumed to be pregnant if their weight gain was over 2 g at E8.5[90]. Thymuses from E14.5 and E17.5 embryos, neonatal, 1-weeks-old pups, and adult mice (older than 6-weeks-old) were harvested, mechanically dissociated with plastic sticks in 1.5-mL centrifuge tubes, and enzymatically digested with 0.2 mg/mL DNase I and 0.2 mg/mL collagenase P in complete DMEM for 20 min at 37˚C with frequent agitation. The cells were resuspended in PBS with 0.5% BSA, filtered through a 70 μm filter, kept on ice, and used flow cytometric analysis as described in the Flow Cytometry section.

Genetic fate mapping – E9.5, neonatal and adult

For genetic fate mapping, timed pregnancies of *Cx3cr1*$^{CreER/CreER}$ male and *ROSA26*$^{LSL\text{-}GFP/LSL\text{-}GFP}$ female mice were set up as described. To label the *Cx3cr1*$^{+}$ erythromyeloid progenitors derived from embryonic yolk sac[8], 4-hydroxytamoxifen (4-OHT from Sigma) was administered i.p. to pregnant females on E9.5 at a dose of 75 μg/g (body weight). To improve the survival of embryos and reduce the risk of abortions, Progesterone (Sigma) was co-injected at a dose of 37.5 μg/g (body weight)[91]. To label the *Cx3cr1*$^{+}$ thymic macrophages in *Cx3cr1*^{CreER} X *ROSA26*$^{LSL\text{-}GFP}$ neonates and adult mice, Tamoxifen (TAM from Sigma) was injected i.p. at a dose of 2 mg/mouse to lactating dams on postnatal day 3 and 4 (P3 and P4) or to adult mice for 2 consecutive days. Thymuses were harvested and analyzed 3 days or 6 weeks after the last injection by flow cytometry.

scRNA-Seq – sorting, library generation, and sequencing

scRNA-Seq was performed at the Genomics Center for Clinical and Biotechnological Applications of NCFB (NYCU, Taipei, Taiwan). Briefly, the thymuses of one female MAFIA and 2 male *Cd11c*^{YFP} mice were harvested and enzymatically digested as described previously. Mononuclear cells were enriched by 57% Percoll PLUS discontinuous centrifugation, washed to remove silica particles, and resuspended at 10^6/mL in PBS with 0.04% BSA. The cell suspensions were filtered through Falcon 35 μm strainer (Corning) and stained with viability dye (PI or DAPI) immediately before sorting. Cell sorting was performed on a FACS Melody sorter (BD Biosciences) running FACS Chorus (BD Biosciences) software in purity mode. 3X10^5 GFP or YFP positive cells under the live/singlet gating were collected into 5 ml round bottom tubes pre-coated with 0.04% BSA in PBS. Sorted cells were washed and resuspended in 300 μL PBS with 0.04% BSA and then filtered again into 1.5-mL DNA LoBind tubes (Eppendorf) through a 35 μm strainer. The viability of the cells was evaluated by Countess II (Invitrogen) and Trypan Blue (ThermoFisher), and samples with cell viability rates higher than 85% were used for encapsulation and library preparation. Single-cell encapsulation and library preparation were performed using Single Cell 3' v3/v3.1 Gene Expression solution (10x Genomics). All the libraries were processed according to the manufacturer's instruction and sequenced on NovaSeq 6000 (Illumina) platform at the NHRI (Zhubei, Taiwan). Post-processing and quality control were performed by the NYCU Genome Center using the CellRanger package (v. 3.0.2, 10x Genomics). Reads were aligned to mm10 reference assembly. Primary assessment with CellRanger reported 9,973 cell-barcodes

with 11,385 median unique molecular identifiers (UMIs, transcripts) per cell and 3,076 median genes per cell sequenced to 71.0% sequencing saturation with 94,260 mean reads per cell for MAFIA mouse sample; 9,801 cell-barcodes with 13,467 median UMIs per cell and 3,211 median genes per cell sequenced to 74.9% sequencing saturation with 119,820 mean reads per cell for the first *Cd11c*^{YFP} mouse sample; 12,938 cell-barcodes with 14,439 median UMIs per cell and 3,199 median genes per cell sequenced to 71.4% sequencing saturation with 108,585 mean reads per cell for the second *Cd11c*^{YFP} mouse sample.

Analysis of scRNA-Seq

Preprocessing

The Scanpy[92] pipeline was used to read the count matrix. Three batches of samples (one from GFP^{+} cells from MAFIA mouse and two from YFP^{+} cells from *Cd11c*^{YFP} mice) were preprocessed independently and integrated later. Cells that expressed <200 genes and genes that were expressed in <3 cells were filtered out. The percentage of mitochondrial genes was calculated -and cells with >10% mitochondrial genes were removed. Cells with >7,000 genes or <1,000 genes were also removed. Read counts were normalized to library size 10,000 and log-transformed with scanpy.pp.log1p function.

Datasets integration and batch effect correction

Read count matrices and spliced/unspliced matrices were merged first. Principal Component Analysis was applied to reduce dimensions to 70. BBKNN[93] was then used to remove batch effects with the scanpy.external.pp.bbknn function with default parameters.

Visualization and clustering

UMAP[94] provided by scanpy was used to visualize data with default parameters. K-nearest neighbor and Leiden clustering were applied sequentially to cluster cells into groups. K-nearest neighbor graph construction was done by scanpy.pp.neighbors with parameters n_neighbors=12 and n_pcs=70. Leiden clustering was then performed by scanpy.tl.leiden with parameter resolution=0.15. To improve UMAP visualization, scanpy.tl.paga was applied, and we trimmed unnecessary graph edges by scanpy.tl.paga with threshold=0.018.

Marker genes and statistics

Wilcoxon rank-sum tests were applied to examine differentially expressed genes. Clusters were selected from the result of Leiden clustering. Differentially expressed genes of a cluster against other clusters were identified by scanpy.tl.rank_genes_groups and scanpy.pl.rank_genes_groups. P-values were collected for each cluster and transformed by negative $\log_{10}$ for better visualization. The top 50 differentially expressed genes were visualized in the figure.

Immunofluorescent staining

Dissected thymus lobes from C57BL/6 mice were cleaned of connective tissue and fixed in 4% paraformaldehyde (Sigma) for 1 h at 4˚C, washed in PBS, submerged in 10% sucrose, and then in 30% sucrose for 12 h each. The tissue was then frozen in Tissue-Tek OCT compound (Sakura Fintek) for cryostat sectioning. 10 or 20 μm thick sections were prepared with CryoStar NX50 (ThermoFisher) on Superfrost PLUS (ThermoScientific) microscope

slides, dried overnight, and stored at -80˚C until used. Before staining, the sections were fixed with acetone (Sigma) at -20˚C for 10 min, air-dried, then blocked with 5% goat serum + 5% donkey serum (both from Jackson Immunoresearch) in PBS for 2 h and stained with primary antibodies: rat monoclonal to MerTK (DS5MMER, eBioscience), rat monoclonal to TIM4 (RMT4-54, Bio-X-Cell) or rabbit polyclonal to Keratin 5 (BioLegend) overnight at 4˚C in a humidified chamber. After washing in PBS, the sections were labeled with goat anti-rat-Alexa Fluor 647 (Invitrogen) or goat anti-rat Cy3 (Jackson Immunoresearch) and donkey anti-rabbit AF647 (Jackson Immunoresearch) secondary antibodies for 2 hours at room temperature, followed by 5 min staining with DAPI. TUNEL Assay was done with the Click-iT Plus TUNEL Assay Alexa Fluor 647 kit (Invitrogen) according to the manufacturer's recommendations. A positive (pre-incubation with DNase I for 30 min at room temperature) and negative (no TdT enzyme) controls were always included. The sections were mounted with 0.1% n-propyl gallate (Sigma) in glycerol (Sigma) and imaged with an AxioObserver 7 (Carl Zeiss) wide-field microscope equipped with Plan Apochromat 20x NA=0.8 objective (Zeiss) and AxioCam 702 mono camera (Zeiss) and controlled by Zen 2.3 Blue (Zeiss) software. Image analysis was performed with Imaris 8.0.2 (Bitplane).

The co-localization scoring for MerTK and TIM4 with TUNEL was done with Imaris 8.2 (Bitplane). TUNEL$^+$ cells were detected with the Spots function, while MerTK$^+$ and TIM4$^+$ cells were detected with the Surface function. Spots that co-localize with Surfaces were identified with the "Find Spots close to

Surface" function of Imaris XT. The threshold for co-localization was set to 5 μm. The results were manually curated so that Spots categorized as "not co-localized" that were: 1) at the edge of the imaging field were excluded from consideration; 2) with clear Surface signal around them were re-categorized as "co-localized". The ratio of co-localized Spots to all Spots was calculated and presented as the co-localization index.

Thymus transplantation

To obtain E15.5 embryos, *ROSA26*^{GFP} homozygous male and C57BL/6 female mice were mated in a cage overnight and separated on the next day. Pregnant mice were sacrificed 15 days later, the viable embryos were harvested, and the thymuses were isolated in ice-cold PBS. C57BL/6 recipients were anesthetized by i.p injection of Ketamine hydrochloride (120 μg/g, Toronto Research Chemicals) and Xylazine hydrochloride (12 μg/g, Sigma). The fur on the left flank was removed, and the left kidney was exposed by cutting the skin, muscle layer, and peritoneum. The kidney capsule was nicked with a G23 needle, and the fetal thymus was pushed into the pocket under the kidney capsule with a G23 needle equipped with a plunger from a spinal needle. After the kidney was re-positioned back into the peritoneal cavity, the peritoneum was sutured, and the skin was stapled with metal clips. Rymadil (Carprofen, 5 μg/g, Zoetis) was given subcutaneously to ease the wound pain, and Trimerin (Sulfadiazine at 0.5 mg/mL + Trimethoprim at 0.1 mg/mL) were given in the drinking water for the first two weeks after the surgery. The metal clips were removed from the skin after the first week, and

the transplanted thymus and recipient's endogenous thymus were harvested and analyzed six weeks after the kidney transplantation.

Statistical analysis

Comparison between groups was made with Prism 6 (GraphPad Software). Comparisons between two groups were carried out with unpaired Student's t-test. When more than two groups were compared, a one-way ANOVA with Tukey correction was used. Differences were considered significant if $p<0.05$.

Data availability

The RNA Sequencing data of thymic macrophages and thymic dendritic cells is available at NCBI Gene Expression Omnibus (GEO) as part of GSE122108 and at www.immgen.org. The single cell RNA sequencing data is deposited at NCBI GEO under accession number GSE185460. The source data underlying Fig. 1g-h, Fig. 3c, f, i, Fig. 4b. f, h, Fig. 6b, d, Fig. 7b, d, e, Fig. S1h, Fig. S3c, and Fig. S4b, d, e, g are provided in the Source Data files. All other data supporting the findings of this study are available within the article and its figures and tables.

Abbreviations:

cDC – classical dendritic cell

DC – dendritic cell

EdU – 5-Ethynyl-2'-deoxyuridine

GO – gene ontology

HSC – hematopoietic stem cell

IFN-I – type I Interferon

IMMGEN – Immunological Genome Consortium

scRNA-Seq – single-cell RNA sequencing

TF – transcription factor

ThyMacs – thymic macrophages

TRA – tissue-restricted antigen

YS – yolk sac

References:

1. Wynn TA, Chawla A, Pollard JW. Macrophage biology in development, homeostasis and disease. Nature. Nature Publishing Group; 2013;496: 445–455. doi:10.1038/nature12034

2. Baratin M, Simon L, Jorquera A, Ghigo C, Dembele D, Nowak J, et al. T Cell Zone Resident Macrophages Silently Dispose of Apoptotic Cells in the Lymph Node. Immunity. Elsevier Inc; 2017;47: 349–362.e5. doi:10.1016/j.immuni.2017.07.019

3. A-Gonzalez N, Castrillo A. Origin and Specialization of Splenic Macrophages. Cellular Immunology. 2018;330: 1–27. doi:10.1016/j.cellimm.2018.05.005

4. Bellomo A, Mondor I, Spinelli L, Lagueyrie M, Stewart BJ, Brouilly N, et al. Reticular Fibroblasts Expressing the Transcription Factor WT1 Define a Stromal Niche that Maintains and Replenishes Splenic Red Pulp Macrophages. Immunity. Elsevier Inc; 2020;53: 127–142.e7. doi:10.1016/j.immuni.2020.06.008

5. van Furth R, Cohn ZA. The origin and kinetics of mononuclear phagocytes. J Exp Med. Rockefeller University Press; 1968;128: 415–435. doi:10.1084/jem.128.3.415

6. Ginhoux F, Guilliams M. Tissue-Resident Macrophage Ontogeny and Homeostasis. Immunity. 2016;44: 439–449. doi:10.1016/j.immuni.2016.02.024

7. Perdiguero EG, Klapproth K, Schulz C, Busch K, Azzoni E, Crozet L, et al. Tissue-resident macrophages originate from yolk-sac-derived erythro-myeloid progenitors. Nat Immunol. Nature Publishing Group; 2015;518: 547–551. doi:10.1038/nature13989

8. Mass E, Ballesteros I, Farlik M, Halbritter F, Günther P, Crozet L, et al.

Specification of tissue-resident macrophages during organogenesis. Science. American Association for the Advancement of Science; 2016;353: aaf4238–aaf4238. doi:10.1126/science.aaf4238

9. Ginhoux F, Greter M, Leboeuf M, Nandi S, See P, Gokhan S, et al. Fate mapping analysis reveals that adult microglia derive from primitive macrophages. Science. 2010;330: 841–845. doi:10.1126/science.1194637

10. Hoeffel G, Wang Y, Greter M, See P, Teo P, Malleret B, et al. Adult Langerhans cells derive predominantly from embryonic fetal liver monocytes with a minor contribution of yolk sac–derived macrophages. J Exp Med. 2012;209: 1167–1181. doi:10.1084/jem.20120340

11. Hoeffel G, Chen J, Lavin Y, Low D, Almeida FF, See P, et al. C-Myb(+) erythro-myeloid progenitor-derived fetal monocytes give rise to adult tissue-resident macrophages. Immunity. 2015;42: 665–678. doi:10.1016/j.immuni.2015.03.011

12. Goldmann T, Wieghofer P, Jordão MJC, Prutek F, Hagemeyer N, Frenzel K, et al. Origin, fate and dynamics of macrophages at central nervous system interfaces. Nat Immunol. 2016;17: 797–805. doi:10.1038/ni.3423

13. Hashimoto D, Chow A, Noizat C, Teo P, Beasley MB, Leboeuf M, et al. Tissue-Resident Macrophages Self-Maintain Locally throughout Adult Life with Minimal Contribution from Circulating Monocytes. Immunity. Elsevier Inc; 2013;38: 792–804. doi:10.1016/j.immuni.2013.04.004

14. Epelman S, Lavine KJ, Beaudin AE, Sojka DK, Carrero JA, Calderon B, et al. Embryonic and Adult-Derived Resident Cardiac Macrophages Are Maintained through Distinct Mechanisms at Steady State and during Inflammation. Immunity. Elsevier Inc; 2014;40: 91–104. doi:10.1016/j.immuni.2013.11.019

15. Sheng J, Ruedl C, Karjalainen K. Most Tissue-Resident Macrophages Except Microglia Are Derived from Fetal Hematopoietic Stem Cells. Immunity. Elsevier Inc; 2015;43: 382–393. doi:10.1016/j.immuni.2015.07.016

16. Liu Z, Gu Y, Chakarov S, Bleriot C, Kwok I, Chen X, et al. Fate Mapping via Ms4a3-Expression History Traces Monocyte-Derived Cells. Cell. Elsevier; 2019;178: 1509–1525.e19. doi:10.1016/j.cell.2019.08.009

17. Ensan S, Li A, Besla R, Degousee N, Cosme J, Roufaiel M, et al. Self-renewing resident arterial macrophages arise from embryonic CX3CR1+ precursors and circulating monocytes immediately after birth. Nat Immunol. Nature Publishing Group; 2015;17: 159–168. doi:10.1038/ni.3343

18. Mondor I, Baratin M, Lagueyrie M, Saro L, Henri S, Gentek R, et al.

Lymphatic Endothelial Cells Are Essential Components of the Subcapsular Sinus Macrophage Niche. Immunity. Elsevier Inc; 2019;50: 1453–1466.e4. doi:10.1016/j.immuni.2019.04.002

19. Molawi K, Wolf Y, Kandalla PK, Favret J, Hagemeyer N, Frenzel K, et al. Progressive replacement of embryo-derived cardiac macrophages with age. J Exp Med. 2014;211: 2151–2158. doi:10.1084/jem.20140639

20. Heidt T, Courties G, Dutta P, Sager HB, Sebas M, Iwamoto Y, et al. Differential Contribution of Monocytes to Heart Macrophages in Steady-State and After Myocardial Infarction. Circulation Research. 2014;115: 284–295. doi:10.1161/CIRCRESAHA.115.303567

21. Yahara Y, Barrientos T, Tang YJ, Puviindran V, Nadesan P, Zhang H, et al. Erythromyeloid progenitors give rise to a population of osteoclasts that contribute to bone homeostasis and repair. Nat Cell Biol. Springer US; 2020;22: 1–28. doi:10.1038/s41556-019-0437-8

22. Jacome-Galarza CE, Percin GI, Muller JT, Mass E, Lazarov T, Eitler J, et al. Developmental origin, functional maintenance and genetic rescue of osteoclasts. Nature. Nature Publishing Group; 2019;568: 541–545. doi:10.1038/s41586-019-1105-7

23. Calderon B, Carrero JA, Ferris ST, Sojka DK, Moore L, Epelman S, et al. The pancreas anatomy conditions the origin and properties of resident macrophages. J Exp Med. 2015;212: 1497–1512. doi:10.1084/jem.20150496

24. Tamoutounour S, Guilliams M, Sanchis FM, Liu H, Terhorst D, Malosse C, et al. Origins and Functional Specialization of Macrophages and of Conventional and Monocyte-Derived Dendritic Cells in Mouse Skin. Immunity. Elsevier Inc; 2013;39: 925–938. doi:10.1016/j.immuni.2013.10.004

25. Bain CC, Bravo-Blas A, Scott CL, Gomez Perdiguero E, Geissmann F, Henri S, et al. Constant replenishment from circulating monocytes maintains the macrophage pool in the intestine of adult mice. Nat Immunol. 2014;15: 929–937. doi:10.1038/ni.2967

26. Sierro F, Evrard M, Rizzetto S, Melino M, Mitchell AJ, Florido M, et al. A Liver Capsular Network of Monocyte-Derived Macrophages Restricts Hepatic Dissemination of Intraperitoneal Bacteria by Neutrophil Recruitment. Immunity. Elsevier Inc; 2017;47: 374–388.e6. doi:10.1016/j.immuni.2017.07.018

27. Mossadegh-Keller N, Gentek R, Gimenez G, Bigot S, Mailfert S, Sieweke MH. Developmental origin and maintenance of distinct testicular macrophage populations. J Exp Med. 2017;214: 2829–2841. doi:10.1084/jem.20170829

28. Lokka E, Lintukorpi L, Cisneros-Montalvo S, Mäkelä J-A, Tyystjärvi S,

Ojasalo V, et al. Generation, localization and functions of macrophages during the development of testis. Nature Communications. Springer US; 2020;11: 1–16. doi:10.1038/s41467-020-18206-0

29. Wang M, Yang Y, Cansever D, Wang Y, Kantores C, Messiaen S, et al. Two populations of self-maintaining monocyte-independent macrophages exist in adult epididymis and testis. PNAS. 2020;118: e2013686117. doi:10.1073/pnas.2013686117/-/DCSupplemental

30. Bain CC, Hawley CA, Garner H, Scott CL, Schridde A, Steers NJ, et al. Long-lived self-renewing bone marrow-derived macrophages displace embryo-derived cells to inhabit adult serous cavities. Nature Communications. Nature Publishing Group; 2016;7: 1–14. doi:10.1038/ncomms11852

31. Surh CD, Sprent J. T-cell apoptosis detected in situ during positive and negative selection in the thymus. Nature. 1994;372: 100–103. doi:10.1038/372100a0

32. Esashi E, Sekiguchi T, Ito H, Koyasu S, Miyajima A. Cutting Edge: A possible role for CD4+ thymic macrophages as professional scavengers of apoptotic thymocytes. Journal of Immunology (Baltimore, Md : 1950). American Association of Immunologists; 2003;171: 2773–2777. doi:10.4049/jimmunol.171.6.2773

33. Liu L-T, Lang Z-F, Li Y, Zhu Y-J, Zhang J-T, Guo S-F, et al. Composition and characteristics of distinct macrophage subpopulations in the mouse thymus. Molecular Medicine Reports. 2013;7: 1850–1854. doi:10.3892/mmr.2013.1448

34. Guerri L, Peguillet I, Geraldo Y, Nabti S, Premel V, Lantz O. Analysis of APC types involved in CD4 tolerance and regulatory T cell generation using reaggregated thymic organ cultures. J Immunol. American Association of Immunologists; 2013;190: 2102–2110. doi:10.4049/jimmunol.1202883

35. Lopes N, Charaix J, Cédile O, Sergé A, Irla M. Lymphotoxin alpha fine-tunes T cell clonal deletion by regulating thymic entry of antigen-presenting cells. Nature Communications. Springer US; 2018;9: 1–16. doi:10.1038/s41467-018-03619-9

36. Kim H-J, Alonzo ES, Dorothee G, Pollard JW, Sant'Angelo DB. Selective depletion of eosinophils or neutrophils in mice impacts the efficiency of apoptotic cell clearance in the thymus. Kim H-J, Alonzo ES, Dorothee G, Pollard JW, Sant'Angelo DB, editors. PLoS ONE. 2010;5: e11439. doi:10.1371/journal.pone.0011439.g010

37. Tacke R, Hilgendorf I, Garner H, Waterborg C, Park K, Nowyhed H, et al. The transcription factor NR4A1 is essential for the development of a novel macrophage subset in the thymus. Sci Rep. 2015;5: 10055. doi:10.1038/srep10055

1182 38. Gautier EL, Shay T, Miller J, Greter M, Jakubzick C, Ivanov S, et al.
1183 Gene-expression profiles and transcriptional regulatory pathways that
1184 underlie the identity and diversity of mouse tissue macrophages. Nat
1185 Immunol. 2012;13: 1118–1128. doi:10.1038/ni.2419

1186 39. Ingersoll MA, Spanbroek R, Lottaz C, Gautier EL, Frankenberger M,
1187 Hoffmann R, et al. Comparison of gene expression profiles between
1188 human and mouse monocyte subsets. Blood. 2010;115: e10–e19.
1189 doi:10.1182/blood-2009-07-235028

1190 40. Wang H, Breed ER, Lee YJ, Qian LJ, Jameson SC, Hogquist KA.
1191 Myeloid cells activate iNKT cells to produce IL-4 in the thymic medulla.
1192 Proc Natl Acad Sci. National Academy of Sciences; 2019;116: 22262–
1193 22268. doi:10.1073/pnas.1910412116

1194 41. Chan CT, Fenn AM, Harder NK, Mindur JE, McAlpine CS, Patel J, et al.
1195 Liver X receptors are required for thymic resilience and T cell output. J
1196 Exp Med. 2020;217: 245–23. doi:10.1084/jem.20200318

1197 42. Wada H, Masuda K, Satoh R, Kakugawa K, Ikawa T, Katsura Y, et al.
1198 Adult T-cell progenitors retain myeloid potential. Nature. Nature
1199 Publishing Group; 2008;452: 768–772. doi:10.1038/nature06839

1200 43. Bell JJ, Bhandoola A. The earliest thymic progenitors for T cells
1201 possess myeloid lineage potential. Nature. 2008;452: 764–767.
1202 doi:10.1038/nature06840

1203 44. Schlenner SM, Madan V, Busch K, Tietz A, LAufle C, Costa C, et al.
1204 Fate Mapping Reveals Separate Origins of T Cells and Myeloid
1205 Lineages in the Thymus. Immunity. Elsevier Ltd; 2010;32: 426–436.
1206 doi:10.1016/j.immuni.2010.03.005

1207 45. Witmer-Pack MD, Hughes DA, Schuler G, Lawson L, McWilliam A,
1208 Inaba K, et al. Identification of macrophages and dendritic cells in the
1209 osteopetrotic (op/op) mouse. J Cell Sci. 1993;104 (Pt 4): 1021–1029.

1210 46. Sasmono RT, Oceandy D, Pollard JW, Tong W, Pavli P, Wainwright BJ,
1211 et al. A macrophage colony-stimulating factor receptor-green
1212 fluorescent protein transgene is expressed throughout the mononuclear
1213 phagocyte system of the mouse. Blood. American Society of
1214 Hematology; 2003;101: 1155–1163. doi:10.1182/blood-2002-02-0569

1215 47. Hume DA. Applications of myeloid-specific promoters in transgenic mice
1216 support in vivo imaging and functional genomics but do not support the
1217 concept of distinct macrophage and dendritic cell lineages or roles in
1218 immunity. Journal of Leukocyte Biology. 2011;89: 525–538.
1219 doi:10.1189/jlb.0810472

1220 48. Taniuchi I, Osato M, Egawa T, Sunshine MJ, Bae SC, Komori T, et al.
1221 Differential requirements for Runx proteins in CD4 repression and
1222 epigenetic silencing during T lymphocyte development. Cell. 2002;111:

621–633. doi:10.1016/s0092-8674(02)01111-x

49. Ebihara T, Song C, Ryu SH, Plougastel-Douglas B, Yang L, Levanon D, et al. Runx3 specifies lineage commitment of innate lymphoid cells. Nat Immunol. Nature Publishing Group; 2015;16: 1124–1133. doi:10.1038/ni.3272

50. Fainaru O, Woolf E, Lotem J, Yarmus M, Brenner O, Goldenberg D, et al. Runx3 regulates mouse TGF-beta-mediated dendritic cell function and its absence results in airway inflammation. EMBO J. John Wiley & Sons, Ltd; 2004;23: 969–979. doi:10.1038/sj.emboj.7600085

51. Kohyama M, Ise W, Edelson BT, Wilker PR, Hildner K, Mejia C, et al. Role for Spi-C in the development of red pulp macrophages and splenic iron homeostasis. Nat Immunol. Nature Publishing Group; 2008;457: 318–321. doi:10.1038/nature07472

52. Haldar M, Kohyama M, So AY-L, KC W, Wu X, Briseño CG, et al. Heme-Mediated SPI-C Induction Promotes Monocyte Differentiation into Iron-Recycling Macrophages. Cell. Elsevier Inc; 2014;156: 1223–1234. doi:10.1016/j.cell.2014.01.069

53. Yona S, Kim K-W, Wolf Y, Mildner A, Varol D, Breker M, et al. Fate Mapping Reveals Origins and Dynamics of Monocytes and Tissue Macrophages under Homeostasis. Immunity. Elsevier; 2013;38: 79–91. doi:10.1016/j.immuni.2012.12.001

54. McCaughtry TM, Wilken MS, Hogquist KA. Thymic emigration revisited. J Exp Med. 2007;204: 2513–2520. doi:10.1084/jem.20070601

55. Lienenklaus S, Cornitescu M, Ziętara N, Łyszkiewicz M, Gekara N, Jabłónska J, et al. Novel reporter mouse reveals constitutive and inflammatory expression of IFN-beta in vivo. J Immunol. American Association of Immunologists; 2009;183: 3229–3236. doi:10.4049/jimmunol.0804277

56. Otero DC, Baker DP, David M. IRF7-dependent IFN-β production in response to RANKL promotes medullary thymic epithelial cell development. J Immunol. American Association of Immunologists; 2013;190: 3289–3298. doi:10.4049/jimmunol.1203086

57. Breed ER, Lee ST, Hogquist KA. Directing T cell fate: How thymic antigen presenting cells coordinate thymocyte selection. Seminars in Cell and Developmental Biology. Elsevier Ltd; 2017;: 1–9. doi:10.1016/j.semcdb.2017.07.045

58. Kurd NS, Lutes LK, Yoon J, Chan SW, Dzhagalov IL, Hoover AR, et al. A role for phagocytosis in inducing cell death during thymocyte negative selection. eLife. 2019;8: 1879–18. doi:10.7554/eLife.48097

59. Morioka S, Perry JSA, Raymond MH, Medina CB, Zhu Y, Zhao L, et al. Efferocytosis induces a novel SLC program to promote glucose uptake

and lactate release. Nature. Springer US; 2018;563: 1–21. doi:10.1038/s41586-018-0735-5

60. Bleriot C, Chakarov S, Ginhoux F. Determinants of Resident Tissue Macrophage Identity and Function. Immunity. Elsevier Inc; 2020;52: 957–970. doi:10.1016/j.immuni.2020.05.014

61. Stritesky GL, Xing Y, Erickson JR, Kalekar LA, Wang X, Mueller DL, et al. Murine thymic selection quantified using a unique method to capture deleted T cells. Proc Natl Acad Sci. 2013;110: 4679–4684. doi:10.1073/pnas.1217532110

62. Baba T, Nakamoto Y, Mukaida N. Crucial Contribution of Thymic Sirp + Conventional Dendritic Cells to Central Tolerance against Blood-Borne Antigens in a CCR2-Dependent Manner. J Immunol. 2009;183: 3053–3063. doi:10.4049/jimmunol.0900438

63. Gallegos AM, Bevan MJ. Central Tolerance to Tissue-specific Antigens Mediated by Direct and Indirect Antigen Presentation. J Exp Med. 2004;200: 1039–1049. doi:10.1084/jem.20041457

64. Koble C, Kyewski B. The thymic medulla: a unique microenvironment for intercellular self-antigen transfer. J Exp Med. 2009;206: 1505–1513. doi:10.1084/jem.20082449

65. Vobořil M, Brabec T, Dobeš J, Šplíchalová I, Březina J, Čepková A, et al. Toll-like receptor signaling in thymic epithelium controls monocyte-derived dendritic cell recruitment and Treg generation. Nature Communications. Springer US; 2020;11: 1–16. doi:10.1038/s41467-020-16081-3

66. Dixit VD. Impact of immune-metabolic interactions on age-related thymic demise and T cell senescence. Semin Immunol. Elsevier Ltd; 2012;24: 321–330. doi:10.1016/j.smim.2012.04.002

67. Rivera-Gonzalez GC, Shook BA, Andrae J, Holtrup B, Bollag K, Betsholtz C, et al. Skin Adipocyte Stem Cell Self-Renewal Is Regulated by a PDGFA/AKT-Signaling Axis. Stem Cell. Elsevier Inc; 2016;19: 738–751. doi:10.1016/j.stem.2016.09.002

68. Olson LE, Soriano P. Increased PDGFRα Activation Disrupts Connective Tissue Development and Drives Systemic Fibrosis. Developmental Cell. Elsevier Ltd; 2009;16: 303–313. doi:10.1016/j.devcel.2008.12.003

69. Satpathy AT, KC W, Albring JC, Edelson BT, Kretzer NM, Bhattacharya D, et al. Zbtb46expression distinguishes classical dendritic cells and their committed progenitors from other immune lineages. J Exp Med. 2012;209: 1135–1152. doi:10.1084/jem.20120030

70. Guilliams M, Mildner A, Yona S. Developmental and Functional Heterogeneity of Monocytes. Immunity. Elsevier Inc; 2018;49: 595–613.

1305 doi:10.1016/j.immuni.2018.10.005

1306 71. Tabula Muris Consortium. Single-cell transcriptomics of 20 mouse
1307 organs creates a Tabula Muris. Nature. Nature Publishing Group;
1308 2018;562: 367–372. doi:10.1038/s41586-018-0590-4

1309 72. Han X, Wang R, Zhou Y, Fei L, Sun H, Lai S, et al. Mapping the Mouse
1310 Cell Atlas by Microwell-Seq. Cell. Elsevier Inc; 2018;172: 1091–
1311 1097.e17. doi:10.1016/j.cell.2018.02.001

1312 73. Tabula Muris Consortium. A single-cell transcriptomic atlas
1313 characterizes ageing tissues in the mouse. Nature. Nature Publishing
1314 Group; 2020;583: 590–595. doi:10.1038/s41586-020-2496-1

1315 74. Kernfeld EM, Genga RMJ, Neherin K, Magaletta ME, Xu P, Maehr R. A
1316 Single-Cell Transcriptomic Atlas of Thymus Organogenesis Resolves
1317 Cell Types and Developmental Maturation. Immunity. Elsevier Inc;
1318 2018;: 1–33. doi:10.1016/j.immuni.2018.04.015

1319 75. Park J-E, Botting RA, Domínguez Conde C, Popescu D-M, Lavaert M,
1320 Kunz DJ, et al. A cell atlas of human thymic development defines T cell
1321 repertoire formation. Science. American Association for the
1322 Advancement of Science; 2020;367: eaay3224–12.
1323 doi:10.1126/science.aay3224

1324 76. Bornstein C, Nevo S, Giladi A, Kadouri N, Pouzolles M, Gerbe F, et al.
1325 Single-cell mapping of the thymic stroma identifies IL-25-producing tuft
1326 epithelial cells. Nature. Springer US; 2018;559: 1–25.
1327 doi:10.1038/s41586-018-0346-1

1328 77. Bautista JL, Cramer NT, Miller CN, Chavez J, Berrios DI, Byrnes LE, et
1329 al. Single-cell transcriptional profiling of human thymic stroma uncovers
1330 novel cellular heterogeneity in the thymic medulla. Nature
1331 Communications. Nature Publishing Group; 2021;12: 1096–15.
1332 doi:10.1038/s41467-021-21346-6

1333 78. Burnett SH, Kershen EJ, Zhang J, Zeng L, Straley SC, Kaplan AM, et
1334 al. Conditional macrophage ablation in transgenic mice expressing a
1335 Fas-based suicide gene. Journal of Leukocyte Biology. Society for
1336 Leukocyte Biology; 2004;75: 612–623. doi:10.1189/jlb.0903442

1337 79. Jung S, Aliberti J, Graemmel P, Sunshine MJ, Kreutzberg GW, Sher A,
1338 et al. Analysis of fractalkine receptor CX(3)CR1 function by targeted
1339 deletion and green fluorescent protein reporter gene insertion. Mol Cell
1340 Biol. 2000;20: 4106–4114.

1341 80. Lindquist RL, Shakhar G, Dudziak D, Wardemann H, Eisenreich T,
1342 Dustin ML, et al. Visualizing dendritic cell networks in vivo. Nat
1343 Immunol. 2004;5: 1243–1250. doi:10.1038/ni1139

1344 81. Faust N, Varas F, Kelly LM, Heck S, Graf T. Insertion of enhanced
1345 green fluorescent protein into the lysozyme gene creates mice with

green fluorescent granulocytes and macrophages. Blood. 2000;96: 719–726.

82. Roesch K, Jadhav AP, Trimarchi JM, Stadler MB, Roska B, Sun BB, et al. The transcriptome of retinal Müller glial cells. J Comp Neurol. 2008;509: 225–238. doi:10.1002/cne.21730

83. Madisen L, Zwingman TA, Sunkin SM, Oh SW, Zariwala HA, Gu H, et al. A robust and high-throughput Cre reporting and characterization system for the whole mouse brain. Nature Neuroscience. Nature Publishing Group; 2009;13: 133–140. doi:10.1038/nn.2467

84. Picelli S, Faridani OR, rklund ASKBO, Winberg GOS, Sagasser S, Sandberg R. Full-length RNA-seq from single cells using Smart-seq2. Nature Protocols. Nature Publishing Group; 2014;9: 171–181. doi:10.1038/nprot.2014.006

85. Picelli S, Björklund ÅK, Faridani OR, Sagasser S, Winberg G, Sandberg R. Smart-seq2 for sensitive full-length transcriptome profiling in single cells. Nat Meth. 2013;10: 1096–1098. doi:10.1038/nmeth.2639

86. Love MI, Huber W, Anders S. Moderated estimation of fold change and dispersion for RNA-seq data with DESeq2. Genome Biol. BioMed Central; 2014;15: 31–21. doi:10.1186/s13059-014-0550-8

87. Schmeier S, Alam T, Essack M, Bajic VB. TcoF-DB v2: update of the database of human and mouse transcription co-factors and transcription factor interactions. Nucleic Acids Res. 2017;45: D145–D150. doi:10.1093/nar/gkw1007

88. Reich M, Liefeld T, Gould J, Lerner J, Tamayo P, Mesirov JP. GenePattern 2.0. Nat Genet. Nature Publishing Group; 2006;38: 500–501. doi:10.1038/ng0506-500

89. Yu G, Wang L-G, Han Y, He Q-Y. clusterProfiler: an R Package for Comparing Biological Themes Among Gene Clusters. OMICS: A Journal of Integrative Biology. Mary Ann Liebert, Inc., publishers; 2012;16: 284–287. doi:10.1089/omi.2011.0118

90. Heyne GW, Plisch EH, Melberg CG, Sandgren EP, Peter JA, Lipinski RJ. A Simple and Reliable Method for Early Pregnancy Detection in Inbred Mice. J Am Assoc Lab Anim Sci. 2015;54: 368–371.

91. Iturri L, Saenz Coronilla J, Lallemand Y, Gomez Perdiguero E. Identification Of Erythromyeloid Progenitors And Their Progeny In The Mouse Embryo By Flow Cytometry. JoVE. 2017;: 1–10. doi:10.3791/55305

92. Wolf FA, Angerer P, Theis FJ. SCANPY: large-scale single-cell gene expression data analysis. Genome Biol. BioMed Central; 2018;19: 15–5. doi:10.1186/s13059-017-1382-0

93. Polański K, Young MD, Miao Z, Meyer KB, Teichmann SA, Park J-E. BBKNN: fast batch alignment of single cell transcriptomes. Bioinformatics. 2019;36: 964–965. doi:10.1093/bioinformatics/btz625#supplementary-data

94. McInnes L, Healy J, Melville J. UMAP: Uniform Manifold Approximation and Projection for Dimension Reduction. ArXiv e-prints. 2018. doi:1802.03426v3

Acknowledgments

We are grateful to the IMMGEN consortium for performing the RNA sequencing of our samples and providing access to its database. We thank the following core facilities at National Yang-Ming Chiao-Tung University: Instrumentation Resource Center for providing access to its sorting and imaging facility and the Animal Facility for mouse husbandry. We are very grateful to Wan-Chun Chang, Bing-Xiu Guo, Chien-Yi Tung, and Kate Hua from the Genomics Center for Clinical and Biotechnological Applications of NCFB (NYCU, Taipei) for help with scRNA-Seq. Special thanks go to Dr. Fang Liao, Academia Sinica, Taipei, for help with cell sorting and for providing the 24G2 hybridoma, and Chang-Feng Chu for technical assistance. We are very grateful to Ms. Su-Hua Jiang at Veterans General Hospital, Taipei, for help with using the irradiator. Some figures were made with BioRender.

This work was supported by the Ministry of Science and Technology (grants # 106-2320-B-010 -026 -MY3, and 107-2320-B-010 -016 -MY3 to IL Dzhagalov and grants # 107-2320-B-010-020, and 108-2628-B-010-005 to CL Hsu), the Yen-Tjing Ling Medical Foundation (grants # CI-107-6 and CI-108-5 to IL Dzhagalov), and the Cancer Progression Research Center (NYCU). The authors declare no competing financial interests.

Author contributions

TA Zhou designed experiments, performed research, analyzed and interpreted data, and wrote the manuscript; HP Hsu and CY Lin performed research, analyzed and interpreted data; YH Tu and HC Huang analyzed the scRNA-Seq data; NJ Chen, JW Tsai, EA Robey, and CL Hsu provided expertise, shared critical reagents, and edited the manuscript; IL Dzhagalov conceptualized the studies, designed experiments, performed research, analyzed, interpreted the data, and wrote the manuscript.

Supplementary figures and tables

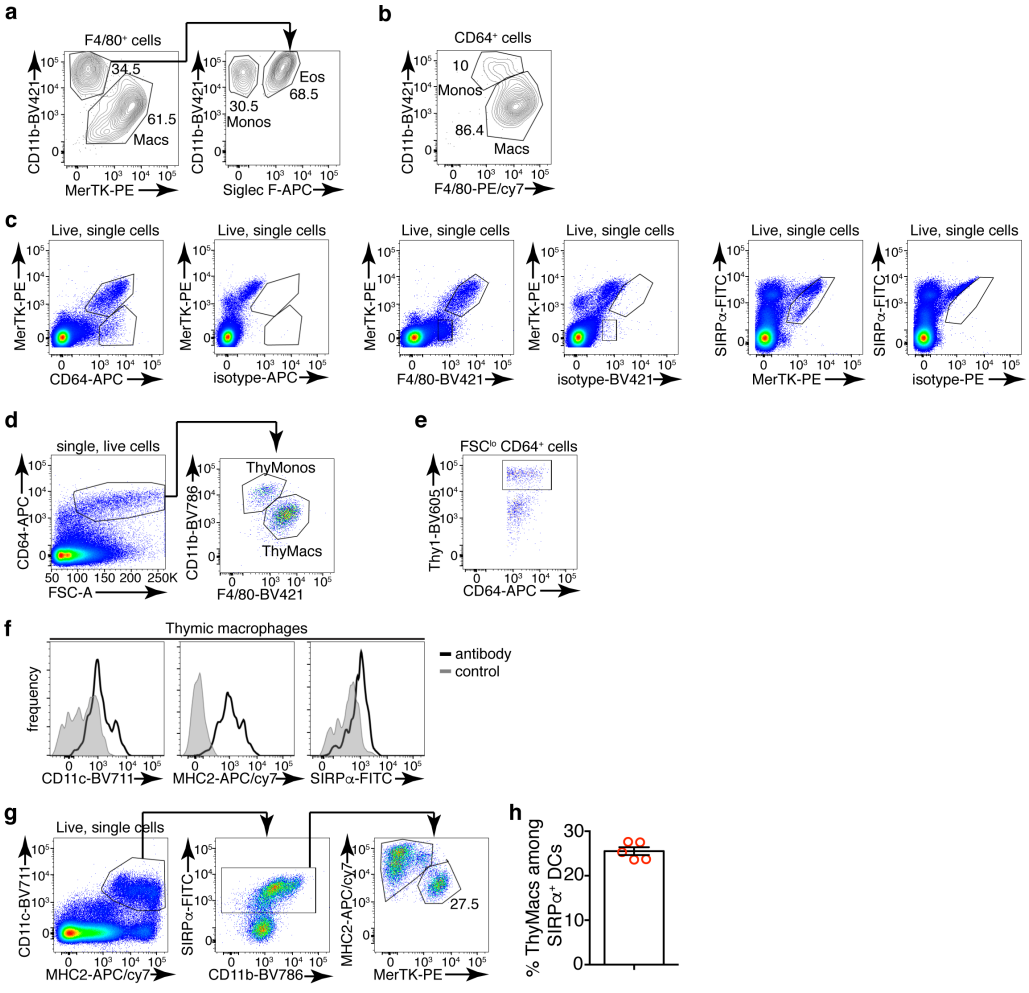

Figure 1 – Figure supplement 1: Phenotype of thymic macrophages and other myeloid cells positive for F4/80 and CD64. a Example flow cytometry plots breaking down F4/80$^+$ cells in the thymus into macrophages (MerTK$^+$), eosinophils (CD11b$^+$MerTK$^-$Siglec F$^+$) and monocytes (CD11b$^+$MerTK$^-$Siglec F$^-$). **b** An example flow cytometry plot dividing CD64+ cells into macrophages (F4/80$^+$CD11b^{lo}) and monocytes (CD11b$^+$F4/80^{lo}). **c** Representative flow cytometry staining of enzymatically digested thymus single-cell suspension for CD64, MerTK, and F4/80 and respective isotype controls. **d** Gating strategy routinely used to identify thymic macrophages as CD64$^+$F4/80$^+$CD11b^{lo}FSC^{hi} cells. **e** Example flow cytometry plots showing that CD64$^+$FSC^{lo} cells include Thy1$^+$ cells (most likely thymocytes). **f** Expression of CD11c, MHC2, and SIRPα on ThyMacs with respective controls. **g** Example flow cytometry plots showing that gating on CD11c$^+$MHC2$^+$ thymus cells, in addition to DCs, also includes macrophages, especially among SIRPα^+ cells. **h** Frequency of MerTK$^+$ cells among CD11c$^+$MHC2$^+$SIRPα^+ cells. The data are mean±SEM from 5 individual mice. Each dot is an individual mouse. The flow cytometry plots are representative of ≥5 individual experiments.

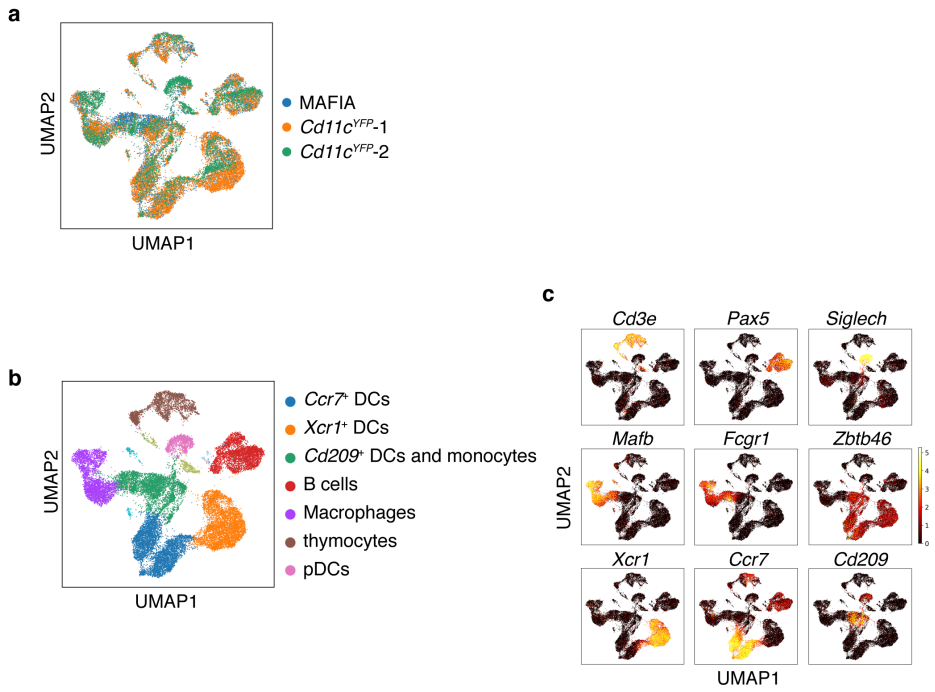

Figure 1 – Figure Supplement 2: UMAP clustering of single-cell RNA-Sequencing (scRNA-Seq) data. a Clustering of the scRNA-Seq data shows that the cells from the three samples (one from GFP$^+$ cells in MAFIA mice and two from YFP$^+$ cells in *Cd11c*^{YFP} mice) overlap considerably. **b** Identification of the clusters from the scRNA-Seq data based on lineage-specific markers. **c** Expression of lineage-specific markers in different clusters.

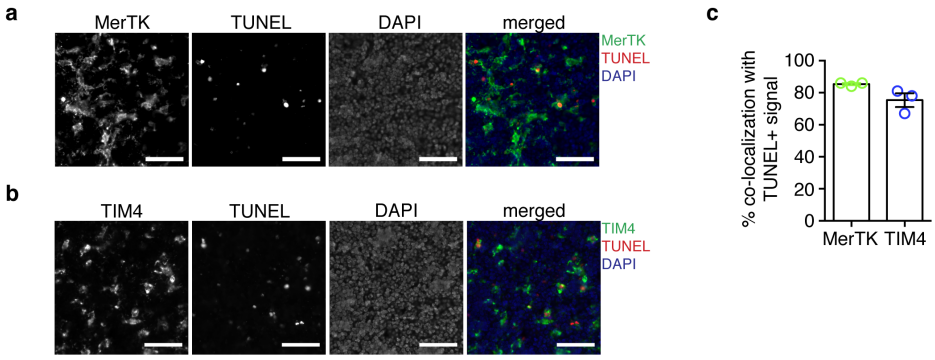

Figure 1 – Figure Supplement 3: Most TUNEL$^+$ apoptotic cells co-localize with thymic macrophages. **a** Example images showing co-localization of TUNEL$^+$ apoptotic cells and MerTK$^+$ ThyMacs. **b** Example images showing co-localization of TUNEL$^+$ apoptotic cells and TIM4$^+$ ThyMacs. Scale bars in **a** and **b** are 50 μm. **c** Frequencies of the co-localization of TUNEL$^+$ signal with MerTK$^+$ and TIM4$^+$ cells. All immunofluorescent images are representative of at least 3 independent repeats. Data in **c** represent mean±SEM. Each dot is an individual mouse.

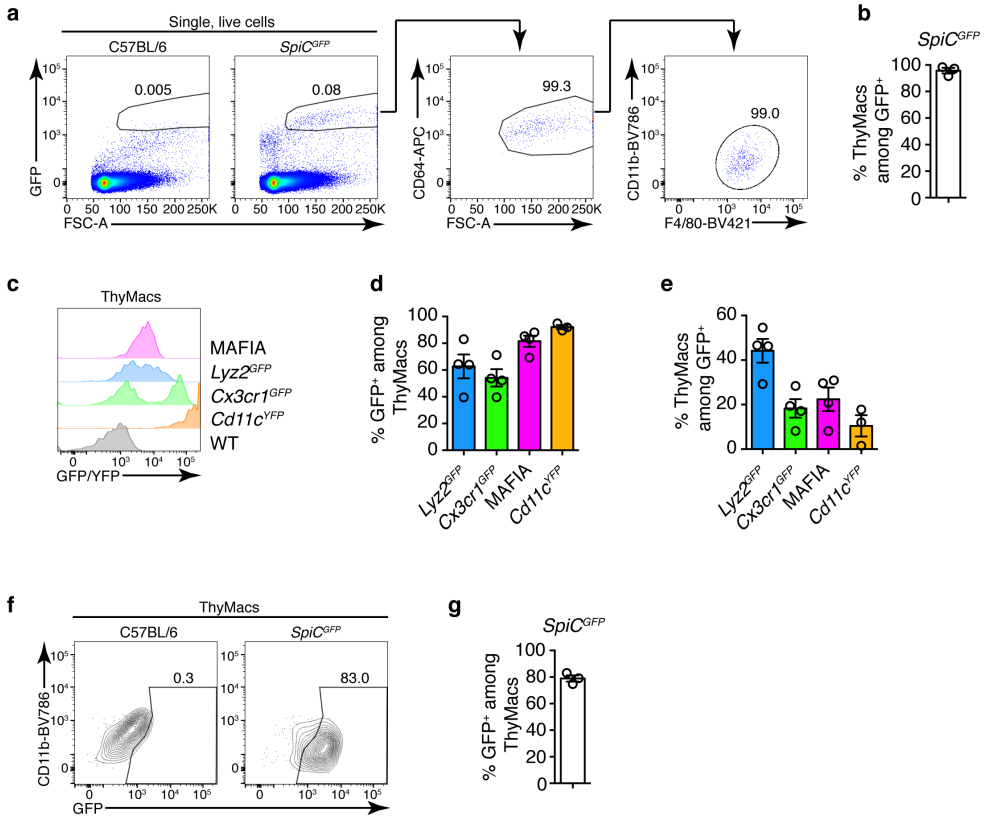

Figure 2 – Figure Supplement 1: Expression of *Spic*^{GFP} marks most thymic macrophages. a Example of the gating strategy to identify ThyMacs among *Spic*$^{GFP+}$ cells. **b** Frequencies of ThyMacs among *Spic*$^{GFP+}$ cells. **c** Representative flow cytometry plots of the expression of four reporter alleles in ThyMacs. **d** Frequencies of GFP/YFP^{+} cells among ThyMacs. **e** Frequencies of ThyMacs among GFP/YFP^{+} cells. **f** Representative flow cytometry plots of the expression of *Spic*^{GFP} in ThyMacs. **g** Frequencies of *Spic*$^{GFP+}$ cells among ThyMacs. All flow cytometry plots are representative of at least 3 independent repeats. Data in **b**, **d**, **e**, and **f** represent mean±SEM. Each dot is an individual mouse. The numbers in the flow cytometry plots are the percent of cells in the respective gate.

Table S1: E**xpression of differentially up-regulated transcription factors in thymic macrophages**

Gene name	ThyMacs	non-ThyMacs
Irf7	3879.32	300.82
Irf8	3528.27	1474.35
Stat1	2403.69	522.04
Dnmt3a	1515.94	647.81
Znxf1	1379.89	635.36
Stat2	1210.35	472.53
Nr1h3	1182.17	147.05
Srebf1	975.09	399.06
Rxra	760.26	298.55
Trps1	746.36	232.48
Runx3	723.14	9.76
Relb	715.53	293.92
Sp100	696.94	324.47
Zbp1	639.19	69.83
Tfec	588.72	74.66
Spic	573.11	34.36
Nfkbie	569.74	226.76
Ncoa4	550.69	249.15
Rest	548.22	269.22
Meis3	530.8	120.91
Bhlhe40	490.59	99.56
Parp12	414.11	126.82
Arid5b	374.03	177.08
Creb5	295.14	47.91
Pparg	276.54	33.24

Figure 2 – Table Supplement 1: Expression of differentially up-regulated transcription factors in thymic macrophages. Transcription factors that were highly expressed in thymic macrophages (>250) and up-

regulated >2-fold in thymic macrophages compared to non-thymic macrophages were listed alphabetically, and the geometric mean of 4 replicates of thymic macrophages (ThyMacs) and two replicates of each of the 9 non-thymic macrophage populations (non-ThyMacs) were recorded. Non-thymic macrophages are: spleen red pulp macrophages, Kupffer cells, bronchoalveolar lavage macrophages, peritoneal cavity macrophages, aorta macrophages, heart macrophages, white adipose tissue macrophages, central nervous system microglia, spinal cord macrophages.

Table S2. **List of the differentially expressed genes among *Timd*4+ thymic macrophages, *Cx3cr1*+ thymic macrophages, and thymic monocytes**

CX3CR1+ ThyMacs		**Tim4+ ThyMacs**		**ThyMonos**	
Gene name	adjusted p-value	Gene name	adjusted p-value	Gene name	adjusted p-value
Ctsz	0	*Hpgd*	0	*Alox5ap*	0
Cd63	0	*Serpinb6a*	0	*S100a6*	0
Pmepa1	0	*Slc40a1*	0	*Ly6c2*	0
Zmynd15	0	*Cd81*	0	*Ifi27l2a*	0
Olfml3	0	*Vcam1*	0	*Fau*	0
Mmp2	0	*Cfp*	0	*Coro1a*	0
AU020206	1.60E-290	*Spic*	0	*Ccr2*	0
Plxnd1	1.59E-285	*Trf*	0	*Rps27*	0
Cst7	8.68E-279	*Actn1*	0	*Tmsb10*	0
Dnase1l3	2.45E-270	*Maf*	0	*Ifitm2*	7.21E-302
Timp2	2.15E-267	*Pld3*	0	*Fxyd5*	6.36E-299
Lgals3bp	8.69E-263	*Il18*	0	*Rps19*	2.04E-292
Pdgfa	6.87E-255	*Mrc1*	0	*Rpl18*	6.50E-291
Mmp14	2.33E-253	*Crip2*	0	*Rpl9*	1.11E-289
Fam46c	9.99E-235	*Tmem65*	0	*Rps23*	1.28E-289
Chst2	1.19E-226	*Igf1*	0	*Napsa*	8.91E-279
Cp	5.36E-225	*Epb41l3*	0	*Ms4a4c*	8.25E-272
Camk1	7.12E-225	*Timd4*	0	*Plac8*	2.10E-270
B2m	1.09E-222	*Blvrb*	0	*Rpl18a*	9.26E-269
Lhfpl2	4.52E-217	*Clec1b*	0	*S100a4*	4.98E-268
Acp5	5.90E-216	*Cd68*	0	*Cd52*	3.67E-267
Lag3	3.91E-213	*Axl*	0	*Rps14*	1.94E-266
Lyz2	1.28E-209	*Paqr9*	3.32E-307	*Ifitm3*	3.19E-263
H2-M2	1.22E-199	*Sdc3*	3.45E-305	*Rpl34*	2.02E-261
Psap	7.26E-198	*Myo9a*	5.59E-305	*Rps27a*	3.67E-260
Gatm	1.33E-192	*Scp2*	3.79E-302	*Rpl36*	1.54E-259
Cpd	1.50E-192	*Selenop*	2.10E-295	*Rps16*	2.55E-258

C3	2.34E-187	*Lrp1*	2.08E-294	*Rpl24*	1.37E-257
Cxcl16	8.11E-183	*Lap3*	1.45E-290	*Rps9*	6.34E-253
Lgals3	1.57E-182	*Marcks*	2.77E-279	*Gpr141*	1.21E-246
Ube2j1	1.63E-180	*Glul*	3.64E-279	*Rpl27a*	3.06E-243
Plxnc1	9.84E-180	*Hebp1*	3.76E-278	*Rpl17*	8.15E-241
Stab1	4.07E-176	*Ear2*	4.53E-276	*Rps24*	1.46E-240
Cyth1	3.27E-163	*Apoc1*	2.49E-275	*Rps13*	2.34E-236
Spsb1	3.96E-163	*Kcna2*	3.72E-275	*Rpl38*	1.95E-226
Blnk	2.35E-162	*Myo10*	9.05E-269	*H2-DMb1*	1.02E-223
Cx3cr1	9.29E-162	*Atp13a2*	2.95E-267	*Rps18*	5.39E-223
Med10	5.25E-161	*Slc1a3*	6.24E-263	*Rpl19*	3.68E-221
Nek6	5.28E-160	*Slco2b1*	1.11E-258	*Rpl8*	2.01E-219
Ptms	1.05E-159	*mt-Nd2*	3.45E-258	*Rpl7a*	4.17E-217
Anxa5	1.10E-156	*Wwp1*	2.16E-253	*Gm34084*	5.23E-216
Gpnmb	1.21E-154	*Aplp2*	4.22E-248	*Rpl13*	2.08E-215
Itgb5	2.78E-154	*Atp8a1*	5.03E-248	*Rpl11*	2.47E-213
Myo5a	1.11E-146	*P2ry13*	3.17E-247	*Rpl35a*	2.13E-210
Runx3	1.81E-146	*Ccdc148*	4.70E-245	*Rpsa*	1.62E-209
Tmem176a	2.34E-144	*Grn*	1.58E-244	*Rpl6*	5.70E-208
Ctss	4.81E-141	*Bank1*	1.82E-239	*Tpt1*	2.63E-206
Sh3pxd2b	9.38E-141	*Mertk*	2.15E-238	*Rack1*	2.14E-203
Rtcb	4.42E-140	*Nr1h3*	1.13E-235	*Rpl23*	6.14E-199
Fam20c	1.91E-139	*Prnp*	2.93E-235	*Rpl26*	7.48E-198
Il2rg	8.84E-138	*Ninj1*	2.42E-234	*Rps6*	6.64E-197
Lpcat2	8.53E-137	*Fcna*	3.33E-233	*Rps10*	2.06E-195
Kynu	8.49E-136	*Csrp1*	1.16E-230	*Ier5*	1.06E-191
Tnfsf13b	8.77E-136	*Rgl1*	7.18E-229	*Rps3*	8.23E-185
Gpr157	1.18E-135	*Lpl*	4.94E-223	*Rpl27*	8.23E-185
Tgfbr1	7.63E-135	*Fam213b*	1.08E-222	*Rps5*	8.36E-185
H2-K1	1.15E-133	*Tcf7l2*	1.26E-222	*Rps7*	3.96E-182
Basp1	1.23E-133	*AB124611*	4.64E-221	*Rps15a*	6.82E-182
Pla2g7	1.80E-132	*Abcc3*	3.28E-216	*Rps11*	1.97E-180
Fth1	4.19E-131	*Fcgrt*	5.79E-216	*Rps4x*	5.07E-180
Ggh	1.85E-126	*Tgm2*	1.88E-215	*Rplp0*	3.09E-177
Adam19	6.94E-126	*Itgad*	5.35E-214	*Ly6i*	8.17E-176
C3ar1	7.35E-125	*Ptgs1*	2.94E-213	*S100a11*	6.23E-175
Ccl12	3.37E-123	*Laptm4a*	1.01E-212	*Atox1*	1.22E-174
Hvcn1	2.51E-121	*Comt*	1.33E-206	*Pim1*	9.56E-174
Anxa3	8.60E-121	*Creg1*	3.24E-205	*Sh3bgrl3*	3.97E-173
Tgfbi	1.88E-120	*Adgre1*	9.67E-205	*Ciita*	7.35E-173
Ctsd	2.73E-117	*Clec12a*	6.33E-204	*Eef1a1*	6.09E-172
Itm2c	5.19E-116	*Tspan4*	7.80E-203	*Rps3a1*	9.09E-168
Tmem119	5.62E-116	*Txn1*	9.13E-203	*Gm2a*	6.07E-165
Rap2a	1.03E-114	*Ctsb*	9.52E-201	*Ptprc*	2.05E-163
Ctsl	4.00E-114	*Mrap*	5.65E-197	*Rpl37*	1.51E-161
Itga6	1.83E-113	*Slc16a9*	5.99E-197	*Rps25*	3.03E-160

B4galnt1	2.45E-113	*Abcg3*	3.83E-196	*H3f3a*	5.92E-159
Fam3c	1.64E-112	*Pla2g15*	4.22E-196	*Btg2*	1.14E-158
Tmem173	1.54E-111	*C1qc*	6.17E-192	*Rpl15*	1.42E-158
Ski	3.59E-111	*Agpat3*	1.68E-191	*Cnn2*	1.09E-156
Anpep	5.85E-111	*Hs6st1*	1.95E-191	*Cdkn1a*	2.57E-156
Gng2	2.37E-110	*Dmpk*	2.15E-191	*Slfn1*	4.83E-155
Nceh1	2.88E-110	*Cd38*	1.79E-190	*Sem1*	4.08E-154
H2-Q7	4.94E-108	*Tmem26*	2.02E-189	*Lsp1*	1.34E-152
Rtn1	1.28E-106	*Slc11a1*	1.05E-188	*Rpl37a*	1.78E-152
Sorl1	1.31E-103	*Cd300a*	1.41E-187	*Rpl22*	3.64E-152
Glipr1	1.22E-102	*Slc7a7*	3.28E-187	*Sirpb1c*	4.81E-152
Gsn	2.00E-102	*Cyb5a*	6.94E-187	*Traf1*	6.97E-152
Afdn	4.54E-102	*Sipa1l1*	7.41E-187	*Emb*	4.22E-151
Ak2	1.11E-101	*Il18bp*	1.48E-186	*Rpl30*	1.32E-147
Ntpcr	2.21E-98	*Cd86*	2.52E-183	*Rps15*	1.14E-146
Scarb2	3.16E-97	*Vamp5*	3.05E-183	*H2-Ab1*	2.84E-145
Creb5	5.41E-97	*Jup*	6.69E-182	*Il1b*	3.05E-145
Gsto1	5.56E-97	*Blvra*	1.30E-178	*Rps28*	4.52E-145
Ncf1	4.26E-96	*Mgst1*	6.48E-178	*Jarid2*	1.82E-143
Ppfia4	4.97E-96	*Tbxas1*	1.47E-177	*Rps26*	1.53E-142
Chchd10	7.77E-96	*Hpgds*	2.04E-177	*Rpl32*	4.21E-142
Gna12	1.23E-95	*Tgfbr2*	2.70E-176	*Pld4*	9.07E-142
Mvb12b	1.80E-95	*Clec4n*	3.52E-175	*Cbfa2t3*	1.54E-141
Rasal3	1.45E-94	*Ms4a7*	5.30E-175	*Rps21*	4.04E-141
Scoc	6.86E-94	*Sirpa*	3.35E-171	*Fgr*	4.04E-141
Cfb	6.00E-93	*Fyn*	2.84E-168	*Rps8*	1.11E-139
Lmna	1.04E-92	*Cadm1*	2.20E-167	*Cd74*	5.34E-138

Figure 5 – Table Supplement 1: List of the differentially expressed genes among *Timd4*$^{+}$ thymic macrophages, *Cx3cr1*$^{+}$ thymic macrophages, and thymic monocytes. The top 100 differentially expressed genes among the three clusters are listed by their negative $\log_{10}$ transformed p-value.